Dear Editor,

I am pleased to resubmit the revised version of our manuscript "No impact of tropospheric ozone on the gross primary productivity of a Belgian pine forest". We appreciated the referees' constructive criticisms, and yours, as associate editor. I have addressed each of the concerns as outlined below.

Associate editor comments:

1. In general, O_3 with the unit ppb should be referred to as mixing ratio instead of concentration.
   Thank you for this remark. We changed this throughout the manuscript.
2. It is unclear to the referee, why the aerodynamic conductance could not be calculated from the data retrieved by the eddy covariance measurements (e.g., u*)? I think a multi-layer approach that considers all conductances of the canopy layers (also the in-canopy aerodynamic conductance) would be more appropriate than a big-leaf approach, but therefore a measured or known vertical profile of the O_3 mixing ratio (and wind speed) has to be known.
   We calculated the aerodynamic conductance based on the friction velocity u and the atmospheric stability function Ψh using the set of coefficients published by Dyer (1974).*
3. Appendix C, equation C3: this equation appears to be wrong. The mixing ratio of O_3 is multiplied by a dimensionless factor given by a ratio of conductances. The resulting unit would be a mixing ratio and not a flux density with the unit nmol m^{-2} s^{-1}. The conventional equation to retrieve F_{st} is (e.g. Gerosa et al., 2005):
   Fst = gst * O_3 (canopy)
   Here, O_3 (canopy) is the O_3 mixing ratio just above the canopy top or at the zero plane displacement height. Note, that this mixing ratio should not be identical to the one used in equation C2 (which is the O_3 mixing ratio at the measurement height). Obviously, the overall results of the manuscript have to be revised if equation C3 was indeed used to derive Fst. The conclusions may change accordingly.
   This was a textual error and is corrected in the revised manuscript. Analyses did not need to be revised because of this.
4. Technical corrections
   We agreed with all of them and changed them accordingly.

Referee #3 comments:

1. Clarification of arguments for using of a GPP model parameterized for days with low O_3 stomatal uptake including detailed discussion/rebuttal.
   We added information about this comment as suggested in the answer to this referee. This can be found at line 242-248 in 'Materials and Methods – 2.5 Detecting O_3 effects on GPP', at line 293-298 in 'Results – 3.3 Ozone effects on GPP' and at line 361-365 in 'Discussion – 4.3 Ozone effects on GPP'.

Referee #4 comments:

1. Justification of assumption that trees behave the same under "low ozone flux" days as if they were never exposed to ozone
   Information about this assumption was added to the manuscript as suggested in the answer to this referee: in 'Materials and Methods – 2.5 Detecting O_3 effects on GPP' from line 249-26,

in 'Results – 3.3 Ozone effects on GPP' from line 299-303 and in 'Discussion – 4.3 Ozone effects on GPP' from line 365-368.

Additional changes:

In addition to the comments, we applied some changes throughout the document to improve the readability. This resulted in a subdivision of Materials and Methods, mainly in the 'Measurements' section. We applied more statistical analyses to endorse our results. This information can be found under 'Materials and Methods - 2.5 Detecting O3 effects on GPP', resulting in additional information in 'Results – 3.3 Ozone effects on GPP' (line 304-318) and in the 'Discussion – 4.3 Ozone effects on GPP' (line 369-374).
We removed table 3 from the manuscript and replaced it by figure 8 which more clearly represents the results. We also reviewed figure 9.

No impact of tropospheric ozone ~~impact~~ on the gross primary uptake~~carbon uptake~~ of~~by~~ a Belgian pine forest

Lore T. Verryckt[1], Maarten Op de Beeck[1], Johan Neirynck[2], Bert Gielen[1], Marilyn Roland[1], and Ivan A. Janssens[1]

[1]Department of Biology, University of Antwerp, Wilrijk, 2610, Belgium

[2]Research Institute for Nature and Forest, Geraardsbergen, 9500, Belgium

Correspondence to: L. Verryckt (lore.verryckt@uantwerpen.be)

Abstract High stomatal ozone (O_3) uptake has been shown to negatively affect crop yields and the growth of tree seedlings. However, little is known about the effect of O_3 on the carbon uptake by mature forest trees. This study investigated the effect of high O_3 events on gross primary productivity (GPP) for a Scots pine stand near Antwerp, Belgium over the period 1998-2013. Stomatal O_3 fluxes were modelled using in situ O_3 mixing ratio measurements and a multiplicative stomatal model, which was parameterised and validated for this Scots pine stand. Ozone-induced GPP reduction is most likely to occur during or shortly after days with high stomatal O_3 uptake. Therefore, a GPP model parameterised for days with low stomatal O_3 uptake rates was used to simulate GPP during periods of high stomatal O_3 uptake. Possible ~~Eventual~~ negative effects of high stomatal O_3 uptake on GPP would then result in an overestimation of GPP by the model during or after high stomatal O_3 uptake events. The O_3 effects on GPP were linked to AOT40 and POD$_1$~~$_y$~~. Although the critical levels for both indices were exceeded in every single year, no significant negative effects of O_3 on GPP were found and no correlations between GPP residuals and AOT40 and POD$_1$~~$_y$~~ were found. Overall, we conclude that no O_3 effects were detected on the carbon uptake by this Scots pine stand.

1 Introduction

Tropospheric ozone (O_3) is a secondary air pollutant that has the potential to negatively affect vegetation, leading to reduced growth and carbon sequestration potential (ICP Vegetation, 2012;Middleton, 1956). Background concentrations of tropospheric O_3 have increased with 36 % since pre-industrial times (IPCC, 2001) and are projected to further increase considerably until about 2050 (IPCC, 2007). Depending on the scenarios, background O_3 levels might either increase or decrease after 2050 (IPCC, 2007).

In recent years, many studies have been conducted to investigate the mechanisms underlying the O_3 impacts on vegetation. Ozone reduces plant growth by altering photosynthetic rates, carbohydrate production, carbon sequestration, carbon allocation, and carbon translocation (Reich and Amundson, 1985;Andersen et al., 1997;Beedlow et al., 2004). Once O_3 enters the leaves through the stomata, it can affect plant growth by direct cellular damage (Mauzerall and Wang, 2001), leading to visible leaf injury and reduced leaf longevity (Noble and Jensen, 1980). In response to O_3, respiratory processes increase, which will also affect the tree's carbon balance (Darall, 1989). Skärby et al. (1987) proved that dark respiration of Scots pine shoots increased after long-term exposure to a low level of O_3. Protective responses, such as compensation (e. g. repair of injured tissue), avoidance

(e. g. stomatal closure), and tolerance (e. g. alteration of metabolic pathways), all consume carbon and, hence, resistance to O_3 damage costs energy. The size of this cost affects the amount of carbon remaining to support growth (Skärby et al., 1998).

To assess the impact of O_3, several indices have been created, e. g. AOT40 (ppb h), the cumulated O_3 mixing ratio in excess of a threshold of 40 ppb, and POD_y, the accumulated O_3 flux above a flux threshold y (nmol m^{-2} s^{-1}). Critical levels, quantitative estimates of exposure to O_3 above which direct adverse effects may occur (CLRTAP, 2015), have been determined for these indices based on O_3 dose-response relationships from fumigation experiments with enhanced O_3 mixing ratios (Karlsson et al., 2004). The magnitude of the O_3 impact on plants depends on the intensity of O_3 exposure, environmental factors influencing both plant photosynthesis and the O_3 flux to plant surfaces, and plant species-specific defensive mechanisms (Musselman and Massman, 1999). Because of the variable plant responses to similar O_3 mixing ratios, the question arises whether widely applicable tolerable limits of O_3 mixing ratio exist (Skärby et al., 1998).

While high stomatal O_3 fluxes have been shown to affect crop yields and the growth of tree seedlings and saplings, ~~it is not sure whether O3 uptake or O3 flux also negatively affects the carbon uptake by mature forest trees. Many studies determined the effect of O3 on seedlings and young trees~~ (e.g. (Buker et al., 2015)), ~~but~~ little is known about the effect on mature trees.When scaling up the results from seedlings to mature trees the resulting data should be viewed with caution, due to differences in energy budgets, canopy:root balances and architecture and carbon allocation patterns (McLaughlin et al., 2007;Chappelka and Samuelson, 1998). In addition to the uncertainties related with the up-scaling from seedlings to mature trees, data from controlled experiments should also be used with caution, because trees can react differently in field conditions (Skärby et al., 1998). The effect of O_3 uptake on carbon uptake under ambient O_3 mixing ratios by trees has hardly been studied in situ. Some studies showed reductions in plant growth due to stomatal O_3 uptake (Zapletal et al., 2011;Fares et al., 2013;Yue and Unger, 2013), while other studies did not show any effect (Zona et al., 2014;Samuelson, 1994). Whether or not an effect of stomatal O_3 uptake was found was species- and site- specific, and there is a clear need for more studies investigating the effect of O_3 on carbon uptake by mature trees in the field (Chappelka and Samuelson, 1998).

In this study~~Here~~ we investigated the effect of ~~high~~ O_3 ~~events~~ at ambient levels on gross primary producti~~o~~vity~~n~~ (GPP) ~~for~~ of a Scots pine stand in Flanders, Belgium over a period of 14 growing seasons between 1998 and 2013. ~~At current ambient O3 levels, c~~Critical levels for both AOT40 and POD1 are already being exceeded in this Scots pine stand (Neirynck et al., 2012),~~. This~~ indicating~~es~~ a potential effect of O_3 on tree productivity already at current ambient levels. ~~that even at current ambient O3 levels tree productivity might be affected. Ozone-induced GPP reduction is most likely to occur during or shortly after days with high stomatal O3 uptake. An effect of stomatal O3 uptake on GPP can be detected when a GPP model parameterised for days with low stomatal O3 uptake rates is extrapolated to high stomatal O3 uptake events – i. e., days where an effect on GPP is assumed - and the model overestimates GPP during these events. This study therefore tests the hypothesis that GPP of the studied pine forest is reduced during or shortly after high stomatal O3 uptake events.~~ To detect O_3 effects on GPP, we adopted a modelling approach that involved simulating GPP with a model with an O_3-damage free parameterisation and evaluating model overestimations of GPP.

2 Materials and methods

2.1 Study area

The study area consisted of a 2-ha Scots pine stand in a 150-ha coniferous/deciduous forest named 'De Inslag', situated in Brasschaat (+51° 18' 33'' N, +04° 31' 14'' E), northeast of the Antwerp agglomeration and east-northeast of the Antwerp harbour (Neirynck et al., 2008). The site has a temperate maritime climate with a mean annual temperature of 11 °C and a mean annual precipitation of 830 mm (Neirynck et al., 2008).

The soil has been classified as Albic Hypoluvic Arenosol (Gielen et al., 2011), a moderately wet sandy soil with a distinct humus and/or iron B-horizon (Janssens et al., 1999). The sandy layer overlays a clay layer which is situated at a depth of 0.7 - 2 m. As a result of the poor drainage groundwater depth is typically high, fluctuating between 0.5 and 2 m (Carrara et al., 2003).

The pine stand was~~trees were~~ planted in 1929 (Neirynck et al., 2008). Until the autumn of 1999, when the forest was thinned,~~In 1995,~~ tree density amounted to 542 trees ha^{-1}. The thinning decreased tree density to ~~In the autumn of 1999, the forest was thinned, which resulted in~~ 376 trees ha^{-1}~~ in 2001~~. Average canpy height is 21.4m (Op de Beeck et al., 2010). With a peak in leaf area index (LAI) of 1.3 ± 0.5 m^2 m^{-2} in 2007 (Op de Beeck et al., 2010) and an average LAI of 1.2 ± 0.5 m^2 m^{-2} in the period 1998-2007, the stand canopy is very sparse. Only two needle-age classes are present: current-year needles and one-year-old needles (Op de Beeck et al., 2010).

The stand is part of the ICP Forests level II and Fluxnet/CarboEurope-IP networks, and is equipped with a 41 m tall instrumentation tower. Measurements of ecosystem CO_2 exchange with the eddy covariance technique and meteorological measurements are being conducted at the site on a continuous basis since 1996 (Gielen et al., 2013).

2.2 Measurements~~: meteorology, O3, GPP, and LAI~~

The period of study covered the period 1998 - 2013, with the years 1999 and 2003 excluded due to poor data quality or coverage.

2.2.1 Meteorology

Air temperature (T_{air}; °C) and humidity (RH; %) were measured with a PT100 and a HMP 230 dew point transmitter (both Vaisala, Finland) in aspirated radiation shields mounted on the tower at 2, 24 and 40 m height. Wind speed (WS, m s^{-1}) was measured with a cup anemometer (LISA, Siggelkow GMBH, Germany) at 24, 32 and 40 m height. Ingoing and outgoing short-wave and long-wave radiation were measured at the top of the tower with a CNR1-radiometer and a CMP6-pyranometer (Kipp and Zonen, the Netherlands). Rainfall was registered by a tipping bucket rain gauge (NINA precipitation pulse transmitter, Siggelkow GMBH, Germany). Both T_{air} and RH were used to calculate vapour pressure deficit (VPD; kPa). Soil temperature (T_{soil}; °C) was measured at 9 cm below the soil surface with temperature probes (Didcot DPS-404, UK). Soil water content (SWC; m^3 m^{-3}) was measured at 25 cm below the soil surface with Time Domain Reflectometers (CS616, Campbell Scientific, UK). Instant SWC was read manually from the Reflectometers every three to 14 days and values were interpolated to obtain daily estimates, taking into account water inputs via precipitation (Gielen et al., 2010). Soil water potential (SWP;

MPa) was derived from the SWC measurements with the model of van Genuchten (van Genuchten, 1980). All meteorological variables (except SWC and rainfall) were measured every 10 seconds and half hourly means were calculated. Data gaps were filled with data from nearby weather stations.

2.2.2 O_3 mixing ratio

The O_3 mixing ratio ($[O_3]$; ppb) was measured at a 10 s resolution above the canopy at 24 m height with an UV Photometric Analyzer (model TEI 49I, Thermo Environmental Instruments) and converted to half hourly averages. Data gaps were filled with $[O_3]$ measurements done at 40 m height. If these were not available, gaps were filled with $[O_3]$ measurements from a nearby weather station from the Flemish Environmental Agency (VMM) at Luchtbal, which is less than 10 km from the site.

2.2.3 Leaf Area Index

A continuous time series with daily LAI values was reconstructed for the pine stand based on the historical data. The general approach was to keep the seasonal pattern measured in 2009 by Op de Beeck et al. (2010) fixed for each year and to scale it year per year to the seasonal maximum LAI (LAI_{max}). LAI_{max} had been measured with the LAI-2050 (LI-COR, Lincoln, Nebraska, USA) in 1997 and 2003 by Gond et al. ((1999) and Konôpka et al. (2005), respectively, and with digital hemispherical photography in 2007 by Op de Beeck et al. (2010). To assure consistency across the time series, measurements were corrected for clumping using a factor 0.83 (Jonckheere et al., 2005). The three measurements of LAI_{max} were interpolated linearly to derive LAI_{max} values for the missing years. The thinning event in 1999 was accounted for by subtracting the removed leaf biomass, determined with allometric relations from Yuste et al. (2005) and specific leaf area measurements from Op de Beeck et al. (2010).

2.2.4 Gross Primary Productivity

Gross primary productivity (µmol C m^{-2} s^{-1}) was derived from net ecosystem exchange (NEE) measured with the eddy covariance technique with the instrumentation and following the standard data quality procedures as explained in (Carrara et al., 2003;Carrara et al., 2004;Gielen et al., 2013). Gross primary productivity was derived by subtracting the modelled total (autotrophic and heterotrophic) ecosystem respiration from the measured NEE. The ecosystem respiration or total carbon loss was modelled with standardised algorithms as presented in Falge et al. (2001). Instant values of GPP were integrated to daily and yearly totals.

~~2.3 Stomatal conductance measurements~~ 2.2.5 Stomatal conductance

Measurements of stomatal conductance to H_2O ($g_{st,\ H2O}$) were done at needle level during the summers of 2007 (Op de Beeck et al., 2010) and 2013 to obtain data for parameterisation of the multiplicative stomatal model used in the calculation of stomatal O_3 fluxes (see sections 2.3 and 2.4). The two summers were marked by quite different environmental conditions: cold and wet in 2007 and warm and dry in 2013. Measurements were carried out with the LI-6400 Gas Exchange System (LI-COR, Lincoln, Nebraska, USA) and included diurnal stomatal courses as well as stomatal responses to PAR, T_{air}, and VPD. Measurements were carried out on sets of three or four live fascicles, i.e. six to eight needles, which were enclosed in the LI-6400's leaf chamber while attached to the tree.

Twenty-six needle sets were measured in total, equally divided between current-year and one-year-old needles. Each needle set was harvested after being measured and hemi-surface needle area was determined in order to express $g_{st,\ H2O}$ on the correct needle area basis. Needle area was derived from needle dimensions (length and width at top, middle, and base), assuming a hemi-circular cross-sectional needle area. Measurements of $g_{st,H2O}$ were converted to stomatal conductance to O_3 (g_{st}) by multiplying $g_{st,H2O}$ with the ratio of the molecular diffusivities of water vapour and O_3 in the air (= 0.61).

~~2.4 Multiplicative stomatal model: description~~

~~Stomatal conductance was modelled using the multiplicative g_{st} model, first described by Jarvis (1976). The model has been developed to calculate species-specific g_{st} according to phenology and environmental conditions (Emberson et al., 2000) and is described in detail in Appendix A.~~

~~We modified the model to make it more applicable for Scots pine. In this modified model (Eq. 1) PAR, T_{air}, VPD, and SWP influence the range between g_{max} and g_{min} instead of g_{max} and zero. This modification was needed, because in the Brasschaat pine forest stomata never completely close, hence g_{st} is never zero (Op de Beeck et al., 2010).~~

~~$g_{st} = g_{max} * f_{phen} * (f_{min} + (1 - f_{min}) * (f_{PAR} * f_T * f_{VPD} * f_{SWP})$ (1)~~

~~Here g_{st} is the stomatal conductance to O_3 and g_{max} is the maximal stomatal conductance to O_3. The functions f_{PHEN}, f_{PAR}, f_T, f_{VPD}, and f_{SWP} represent the modification of g_{max} by, respectively, phenology, PAR, T_{air}, VPD, and SWP. The function f_{min} is the ratio of g_{min} and g_{max} where g_{min} is the minimal stomatal conductance to O_3 (see Appendix A for more detailed information). Impaired stomatal aperture mechanisms (stomatal sluggishness) due to O_3exposure (Paoletti and Grulke, 2010) were not included in the model development.~~

~~2.5 Canopy model~~2.3 Calculation of stomatal O_3 fluxes

~~We applied a canopy model to scale up g_{st}, measured at leaf level, to the canopy level. The canopy model consists of different horizontal leaf layers and includes a radiation transfer model (Goudriaan, 1977), a solar elevation model (Campbell and Norman, 1998) and the modified multiplicative stomatal model (Emberson et al., 2000). The model is described in detail in Appendix C.~~

~~The model calculates half-hourly totals of the total, stomatal, and non-stomatal O_3 fluxes based on the following input variables: day of year, hour, Rg, T_{air}, VPD, SWP, O_3 mixing ratio above the canopy (24m), LAI, and friction velocity u*. The total O_3 flux (nmol m^{-2} s^{-1}) for the whole canopy was the product of O_3 mixing ratio (ppb) and g_{tot} (mol (m^2 ground area^{-1}) s^{-1}) (Musselman and Massman, 1999). This last parameter was calculated with an electrical model (Eq. 2).~~

Stomatal O_3 fluxes were calculated at a half-hourly resolution from continuous series of half-hourly [O_3] and meteorology and daily LAI with an electric analog model built from three resistances in series:

$$R_{tot} = R_{aero} + R_{bl} + R_{can} \qquad (1)$$

where R_{tot} is the total resistance to O_3, R_{aero} is the aerodynamic resistance to O_3, R_{bl} is the quasi-laminar boundary layer resistance to O_3, and R_{can} is the canopy resistance to O_3 (all expressed in s m^{-1}).

~~$g_{tot} = (\frac{1}{g_{aero}} + \frac{1}{g_{bl}} + \frac{1}{g_{can}})^{-1} \qquad (2)$~~

~~where g_{tot} is the total conductance to O_3 (mol (m^2 ground area^{-1}) s^{-1}); g_{aero} is the aerodynamic conductance; g_{bl} is the boundary layer conductance to O_3; g_{can} is the canopy conductance.~~

~~The aerodynamic conductance g_{aero} was calculated with the following formula (Grünhage, 2002):~~

~~$g_{aero} = \frac{1}{\kappa u^*} [\ln(\frac{z-d}{z_0}) - \Psi_h\left(\frac{z-d}{L}\right) + \Psi_h(\frac{z_0}{L})] \qquad (3)$~~

~~where the von Karman constant κ = 0.43; u* (m s-1) is the friction velocity; L is the obukov length; z is the height at which the O_3 mixing ratio was measured ; d is the zero plane displacement (Appendix C); z_0 is the momentum roughness parameter (Appendix C) ; Ψh is the atmospheric stability function calculated using the set of coefficients published by Dyer (1974) and is described in detail in Appendix C.~~

The aerodynamic resistance was calculated following (Grünhage, 2002) with:

$$R_{aero} = \frac{1}{\kappa u^*} [\ln(\frac{z-d}{z_0}) - \Psi_h\left(\frac{z-d}{L}\right) + \Psi_h(\frac{z_0}{L})] \qquad (2)$$

where κ is the von Karman constant (0.43), u* (m s^{-1}) is the friction velocity, L is the Obukhov length, z is the $[O_3]$ measurement height (24 m), d is the zero plane displacement (= 0.1 h), z_0 is the momentum roughness parameter (= 0.65 h), h is the canopy height, and Ψ_h is the atmospheric stability function. This function is calculated using the set of coefficients published by Dyer (1974):

- for unstable atmospheric stratification (L < 0m)

$$\Psi_h = 2 * \ln[\frac{1}{\varphi_h(\zeta)} + 1] \qquad (3)$$

$$\varphi_h = (1 - 16 * \zeta)^{-0.5} \qquad (4)$$

$$\zeta = \frac{z-d}{L} \text{ with } z = z_2 = z_{ref,T} \text{ and } z = z_1 = d + z_0 \qquad (5)$$

- for stable atmospheric stratification (L > 0m):

$$\Psi_h = -5 * \zeta \qquad (6)$$

$$\zeta = \frac{z-d}{L} \text{ with } z = z_2 = z_{ref,T} \text{ and } z = z_1 = d + z_0 \qquad (7)$$

- for neutral atmospheric stratification (|L| → ∞):

$$\Psi_h = 0 \qquad (8)$$

~~The boundary layer conductance to O_3 was calculated with the following formula (Baldocchi et al., 1987):~~

~~$g_{bl} = \frac{\kappa * u^*}{2 * \frac{Sc^{\frac{2}{3}}}{Pr}} * 44.64 \qquad (4)$~~

~~where κ is the von Karman constant (0.43); u* (m s^{-1}) is the friction velocity, which is derived from the measured momentum fluxes; Sc is the Schmidt number (1.07 for O_3); Pr is the Prandtl number (0.72 for O_3); 44.64 mol m^{-3} is the molar density of air (at an air pressure of 101.3 kPa and an air temperature of 0°C), and is applied for converting the unit of g_{bl} from m s^{-1} to mol m^{-2} s^{-1}.~~

The quasi-laminar boundary layer resistance was calculated following (Baldocchi et al., 1987) with:

$$R_{bl} = \frac{2}{\kappa * u^*}\left(\frac{Sc}{Pr}\right)^{2/3} \qquad (9)$$

where κ is the von Karman constant (0.43), u* (m s^{-1}) is the friction velocity, which is derived from the measured momentum fluxes, Sc is the Schmidt number (1.07 for O_3), and Pr is the Prandtl number (0.72 for O_3).

~~The canopy conductance consisted of a stomatal and a non-stomatal component. Since the stomatal component varies throughout the canopy, the canopy was divided into eight sublayers so that the leaves were evenly distributed between the horizontal layers. Dividing the canopy into sufficient sublayers was necessary in order to model fluxes well. Eight sublayers were considered to be sufficient, as indicated in a sensitivity test with more and less sublayers. For each leaf layer, the model calculates g_{st} for sunlit and shaded needles, taking the solar elevation angle into account. Non-stomatal conductance was assumed to be constant over the canopy and was set to 0.16 mol m^{-2} s^{-1}. This value was derived from long-term O_3 flux measurements in Brasschaat (Neirynck et al., 2012).~~

~~The stomatal and non-stomatal O_3 fluxes (nmol m^{-2} s^{-1}) were calculated by multiplying the proportion of g_{st} and g_{ns} of the canopy per ground area with the O_3 mixing ratio.~~

~~These obtained half-hourly fluxes were aggregated to daily fluxes. These daily fluxes were averaged in order to know the average daily O_3 uptake by the canopy for the different years. The ratio F_{st}/F_{tot} was calculated and this gives an indication of the contribution of the stomatal O_3 flux to the total O_3 flux.~~

The canopy resistance was calculated from a stomatal resistance (R_{st}) and a non-stomatal resistance (R_{nst}), mounted in parallel:

$$R_{can} = \left(\frac{1}{R_{st}} + \frac{1}{R_{nst}}\right)^{-1} \qquad (10)$$

The stomatal resistance R_{st} was calculated with an algorithm that divides the pine canopy into eight horizontal leaf layers, with LAI being divided equally between the layers, and that simulates the transfer of radiation through the layered canopy. The algorithm then calculates the stomatal resistance for the sunlit and shaded area fraction of each leaf layer with the multiplicative stomatal model described by Jarvis (1976) and reformulated by (Emberson et al., 2000). Resistance values are then integrated over all layers to obtain canopy level R_{st}. The algorithm is explained in more detail in Op de Beeck et al. (2010). The version of the multiplicative stomatal model used in this study is described in detail in Appendix A. This model was given a site-specific parameterisation as explained in section 2.4.

The non-stomatal resistance R_{nst} was assumed to be constant in time and set to 279 s m^{-1}. This value was derived from long-term O_3 flux measurements in Brasschaat (Neirynck et al., 2012).

Total and stomatal O_3 fluxes (F_{tot} and F_{st}; nmol m^{-2} s^{-1}) were calculated on a halfhourly basis with:

$$F_{tot} = 44.64\,\frac{[O_3]}{R_{tot}} \qquad (11)$$

$$F_{st} = F_{tot}\,\frac{R_{can}}{R_{st}} \qquad (12)$$

where 44.64 is the molar density of air in mol m^{-3} at an air pressure of 101.3 kPa and an air temperature of 0°C, used here to convert flux units from m s^{-1} to mol m^{-2} s^{-1}. Half-hourly fluxes were aggregated to daily and yearly values.

2.4 Parameterisation and validation of the multiplicative stomatal model

~~For the optimisation of the parameters of the different functions in the model, we assumed that the phenology function was 1. This was deemed a fair assumption, because gst,H2O was measured on mature needles in the summer (July/August 2007 and 2013), in the middle of the growing season.~~

The multiplicative stomatal model was parameterised and validated against the dataset of g_{st} measurements collected at the site. This~~e~~ dataset ~~,~~ included besides measured g_{st} also~~ing measured gst,~~ PAR, T_{air}, VPD, and SWP, and was split into a parameterisation set and a validation set ~~two subsets~~ by grouping the odd and even rows ~~for~~ of data ~~sorted~~ after being ranked by PAR. ~~One set was then used for parameterisation, the other for validation. The stomatal model was parameterised using the computer program Matlab (version 2013a).~~ Parameterisation was done by optimising ~~The optimisation of all~~ model parameters ~~was done~~ with the function ‘lsqcurvefit’ in Matlab (Matlab and Statistics Toolbox Release 2013a), ~~. It~~ which finds the best parameter values~~,~~ starting ~~with~~ from an initial value and which~~, to best fit the function of the stomatal model to measured gst and~~ can ~~thus~~ be used to fit ~~a~~ nonlinear functions with more than two independent variables. The~~All~~ parameters of the boundary functions f_{PAR}, f_{Tair}, f_{VPD}, and f_{SWP} were optimised separately, ~~with~~ starting from initial values that were estimated visually from plots of g_{st} versus each of the input variables (PAR, T_{air}, VPD, and SWP). The phenology function f_{PHEN} was set to 1, since g_{st} had been measured on mature needles only.~~the functions to the dataset.~~

~~2.4.2 Multiplicative stomatal model: model evaluation~~

The parameterised model was then tested against the validation dataset. ~~Measured g_{st} values were plotted against the modelled g_{st} values.~~ Model performance was evaluated with the linear regression~~A linear function~~ $y=ax+b$ ~~was~~ fitted to the plot of measured versus modelled g_{st}, and with the following set of performance~~, where ‘a’ should be not 170 significantly different from one (p > 0.05) and ‘b’ should be not significantly different from zero (p > 0.05) for both parameterisation and validation dataset. We evaluated the model performance with the following~~ statistics: the coefficient of determination ~~or R squared~~ (R^2) ~~as a goodness-of-fit measure and error-based measures including~~ , mean bias (MB), relative mean error (RME), Willmott’s index of agreement (d), model efficiency

(ME), and root mean squared error (RMSE)~~,~~ and its systematic ($RMSE_s$) and unsystematic component ($RMSE_u$). These statistics are explained briefly ~~I~~in Appendix B~~ these 175 error-based statistics are explained~~. To evaluate visually the goodness-of-fit of each boundary function, modelled g_{st} was plotted versus each of the

~~The measured g_{st} was plotted in function of the different~~ input variables~~ (PAR, T_{air}, VPD, and SWP) and the boundary function of each plot was fitted. This was done in order to test how well the obtained parameter values were estimated in function of the measured g_{st}.~~ and the corresponding boundary function added to the scatter plot.

~~2.5 Canopy model~~

~~We applied a canopy model to scale up g_{st}, measured at leaf level, to the canopy level. The canopy model consists of different horizontal leaf layers and includes a radiation transfer model (Goudriaan, 1977), a solar elevation model (Campbell and Norman, 1998) and the modified multiplicative stomatal model (Emberson et al., 2000). The model is described in detail in Appendix C.~~

~~The model calculates half-hourly totals of the total, stomatal, and non-stomatal O_3 fluxes based on the following input variables: day of year, hour, Rg, T_{air}, VPD, SWP, O_3 mixing ratio above the canopy (24m), LAI, and friction velocity u*. The total O_3 flux (nmol m^{-2} s^{-1}) for the whole canopy was the product of O_3 mixing ratio (ppb) and g_{tot} (mol (m^2 ground area^{-1}) s^{-1}) (Musselman and Massman, 1999). This last parameter was calculated with an electrical model (Eq. 2).~~

~~$g_{tot} = \left(\frac{1}{g_{aero}} + \frac{1}{g_{bl}} + \frac{1}{g_{can}}\right)^{-1}$ (2)~~

~~where g_{tot} is the total conductance to O_3 (mol (m^2 ground area^{-1}) s^{-1}); g_{aero} is the aerodynamic conductance; g_{bl} is the boundary layer conductance to O_3; g_{can} is the canopy conductance.~~

~~The aerodynamic conductance g_{aero} was calculated with the following formula (Grünhage, 2002):~~

~~$g_{aero} = \frac{1}{\kappa u^*}\left[\ln\left(\frac{z-d}{z_0}\right) - \Psi_h\left(\frac{z-d}{L}\right) + \Psi_h\left(\frac{z_0}{L}\right)\right]$ (3)~~

~~where the von Karman constant κ = 0.43; u* (m s-1) is the friction velocity; L is the obukov length; z is the height at which the O_3 mixing ratio was measured ; d is the zero plane displacement (Appendix C); z_0 is the momentum roughness parameter (Appendix C) ; Ψh is the atmospheric stability function calculated using the set of coefficients published by Dyer (1974) and is described in detail in Appendix C.~~

~~The boundary layer conductance to O_3 was calculated with the following formula (Baldocchi et al., 1987):~~

~~$g_{bl} = \frac{\kappa * u^*}{2 * \left(\frac{Sc}{Pr}\right)^{\frac{2}{3}}} * 44.64$ (4)~~

~~where κ is the von Karman constant (0.43); u* (m s^{-1}) is the friction velocity, which is derived from the measured momentum fluxes; Sc is the Schmidt number (1.07 for O_3); Pr is the Prandtl number (0.72 for O_3); 44.64 mol m^{-3}~~

~~is the molar density of air (at an air pressure of 101.3 kPa and an air temperature of 0°C), and is applied for converting the unit of g_{bl} from m s^{-1} to mol m^{-2} s^{-1}.~~

~~The canopy conductance consisted of a stomatal and a non-stomatal component. Since the stomatal component varies throughout the canopy, the canopy was divided into eight sublayers so that the leaves were evenly distributed between the horizontal layers. Dividing the canopy into sufficient sublayers was necessary in order to model fluxes well. Eight sublayers were considered to be sufficient, as indicated in a sensitivity test with more and less sublayers. For each leaf layer, the model calculates g_{st} for sunlit and shaded needles, taking the solar elevation angle into account. Non-stomatal conductance was assumed to be constant over the canopy and was set to 0.16 mol m^{-2} s^{-1}. This value was derived from long-term O_3 flux measurements in Brasschaat (Neirynck et al., 2012).~~

~~The stomatal and non-stomatal O_3 fluxes (nmol m^{-2} s^{-1}) were calculated by multiplying the proportion of g_{st} and g_{ns} of the canopy per ground area with the O_3 mixing ratio.~~

~~These obtained half-hourly fluxes were aggregated to daily fluxes. These daily fluxes were averaged in order to know the average daily O_3 uptake by the canopy for the different years. The ratio F_{st}/F_{tot} was calculated and this gives an indication of the contribution of the stomatal O_3 flux to the total O_3 flux.~~

~~2.6 Ozone effects~~2.5 Detecting O_3 effects on GPP

We adopted a modelling approach to detect possible O_3 effects on GPP. Under the assumption that O_3-induced GPP reduction is most likely to occur during and shortly after days of high stomatal O_3 fluxes, we parameterised a GPP model against a dataset from which such days where removed and then simulated daily and growing season GPP with this supposedly O_3-damage free model. A reduction of GPP due to O_3 would become apparent as a model overestimation of daily GPP for the days on which an O_3 effects was assumed, and possibly also as an overestimation of growing season GPP.

We used as GPPmodel a~~A~~ feed-forward back propagation Artificial Neural Network (ANN) in Matlab (Matlab and Statistics Toolbox Release 2013a). The ANN contained 10 nodes organised in 1 layer, which came out as the best performing network after comparing networks containing different number of nodes and/or layers (data not shown). The default settings of the Matlab Neural Network Toolbox were used. A normalisation process was applied for training and testing the data: data were scaled to [-1 1] based on the lowest and highest value in the dataset. The daily GPP data were used as dependent target variable in the ANN. The input variables were year, day of year, T_{min}, T_{max}, T_{mean}, average VPD, SWC, R_g, average T_{soil}, and average WS. Daily totals of the variables were used, with the exception of VPD, T_{soil}, and WS for which daily averaged values were used.

To obtain an O_3-damage free GPP model, days for which an O_3 effect on GPP was expected were removed from the dataset. These were taken as the days with the 2%, 5% or 10% highest stomatal O_3 fluxes. Because the results for a 2% and 10% cut-off were equal to those for a 5% cut-off, we report only results for a 5% cut-off. The model was trained with 2/3 of the remaining dataset, while the other 1/3 was used to test the model. This O_3-damage free model was then run with the full dataset. ~~The absolute and relative differences in GPP simulated over the growing season between EC derived and modelled values were calculated, to investigate whether or not there was a reduction of GPP.~~

~~The relation between the residuals of total GPP and both AOT40, POD_1 and POD_2 was examined. Therefore, a linear fit between the residuals and the indices was made. A significant negative correlation would exist if the slope is significant different from 0 ($p < 0.05$) and intercept is not significant different from 0 ($p > 0.05$). These yearly GPP residuals were also plotted to the stomatal O_3 flux to investigate their relation and a linear fit was made of which the significance was tested. If GP was increasingly overestimated in the presence of higher stomatal O_3 fluxes, this would indicate a deleterious O_3 effect.~~

~~Ozone effects possibly appear and last during a period of several days after the O_3 peaks, and as a result they will not be detected in the above analyses. Due to these possibly lag effects of O_3, the above analyses were repeated, but now excluding the days with high stomatal O_3 uptake along with the two subsequent days removed from the training and testing datasets.~~Model overestimation of daily GPP was evaluated (1) from the linear regression on the data of measured versus modelled GPP for the days on which an O_3 effect was assumed, testing whether the regression slope and intercept were different from 1 and 0, and (2) by comparing measured and modelled daily GPP for these days by means of a paired-samples t-test or a Wilcoxon signed-rank test if differences were not normally distributed (Shapiro-Wilk test). A significant outcome of this test in combination with a regression slope significantly lower than 1 (and an intercept not different from 0) would together point to a significant overestimation of GPP. Furthermore, (3) the regression slope and intercept were compared with the slope and intercept of the regression fitted to the dataset used to train and test the GPP model. This was done to evaluate whether GPP estimations for the days on which we assumed an O_3 effect were, in relative terms, significantly higher than GPP estimations for the days used for model training and testing. This would become apparent as a significantly lower slope (with an intercept no different from 0). Model overestimation of growing season GPP was evaluated with the first two tests above on the growing season data. Additionally, the residuals of growing season GPP (model - measurement) were plotted against AOT40, POD_1, and total growing season stomatal O_3 uptake, and linear regression lines fitted. It was tested whether regression slope and intercept were significantly different from 0 to assess the presence of a statistically significant O_3 dose response relationship.

Since O_3 effects might last several days after a peak of O_3 exposure, they might not be detected with the model parameterised as explained above. To account for such a sustained O_3 effect, the modelling was repeated, now not only excluding the days with the highest stomatal O_3 fluxes from the dataset for model training but also the two following days. The results were evaluated with the same statistical tests as mentioned above.

High O_3 events are often coupled with specific meteorological conditions, i.e. high radiation and air temperatures. Since the dataset for model training had been compiled by removing the days with the highest stomatal O_3 fluxes, it was not unlikely that these conditions were underrepresented in the training dataset. If so, this could induce a bias in the model response to radiation and temperature and possibly result in overestimations of GPP for the days on which an O_3 effect was expected, which we then might wrongly attribute to O_3. To evaluate the risk for such model bias, we compared the frequency distribution and range of radiation, T_{min}, T_{max}, T_{mean}, and also VPD between the training dataset and the dataset with the days on which we expected an O_3 effect.

One of the assumptions in our approach is that O_3 effects on GPP only last on the short term, i.e. just a few days, and are hence not carried over. The presence of a carry-over effect would compromise the validity of our approach. We can rule out a carry-over effect by testing whether trees exposed to low stomatal O_3 fluxes late in the growing season behave in the same way as when exposed to similar low O_3 fluxes early in the growing season. To test this, we compiled a dataset that contained per growing season only the days after the first major peak of stomatal O_3 flux in the growing season. From this period, we further selected only the days with low stomatal O_3 fluxes for which moreover no short-term O_3 effect was expected. In other words, we excluded the days with a peak of stomatal O_3 flux plus the six following days. We trained the GPP model with these data and then predicted GPP for the days before the first major O_3 peak in each growing season. If a carry-over effect would be present, at least an effect induced during the first major O_3 flux peak, it would be somehow included in the trained model. This would then underestimate GPP for the days before each first major O_3 peak, where a carry-over effect has assumptively not yet occurred. Model underestimation of GPP was evaluated from a linear regression on the data of measured versus modelled GPP, testing whether the regression slope and intercept were different from 1 and 0. This slope and intercept were also compared with the slope and intercept of the regression line fitted to the training data. Also, measured and modelled GPP were compared with a paired-samples t-test or a Wilcoxon signed-rank test if differences were not normally distributed (Shapiro-Wilk test).

All statistics were performed with R 3.2.3 (R Core Team, 2015) at a significance level of $p = 0.05$.

3 Results

3.1 Measurements: meteorology, GPP, and LAI

Figure 1 shows a~~A~~ fingerprint of the multi-annual average diel and seasonal pattern ~~in the measured data is shown in Fig. 1.~~of the main meteorological variables, being T_{air}, incoming global radiation (R_g) and VPD, and measured GPP. This figure gives a good overview of how meteorology and GPP typically changed over time in this forest; interannual anomalies from the average patterns can be found in Fig. S1. Distinct daily and seasonal patterns can be observed for T_{air}, R_g, and VPD, reaching highest values in summer, in the afternoon. Similar patterns can also be observed in GPP, which basically follows the pattern of R_g. As seen in Fig. 1, the photosynthetic period extends, on average, from day of year 115 (end of April) till day of year 300 (end of October). The ~~precipitation and SWP~~ time series of precipitation and SWP are provided in Fig. 2, while ~~changes~~ the seasonal ~~in~~ LAI courses ~~over time~~ are shown for each year in Fig. 3. The yearly maximum LAI ranged from 1.4 to 1.9 m^2 m^{-2}. The thinning of the forest in 1999 can clearly be observed in the LAI pattern. After the thinning, the canopy never fully closed.

3.2 Multiplicative stomatal model and simulated O_3 fluxes

The ~~best fitting parameter values for the multiplicative stomatal model~~ optimized parameter values of the model are presented in Table 1. The different statistics to evaluate the model performance are presented in Table 2 and this for both the parameterisation and validation dataset. For the parameterisation dataset, the measured data were plotted against modelled g_{st} and plotted in Fig. 4A. The slope of the linear fit was not significantly different from 1 ($p > 0.05$) and the intercept was not significantly different from 0 ($p > 0.05$). Model evaluation for the validation dataset was equally good as for the parameterisation dataset (Table 2). Also in the linear fit for the validation set (Fig. 4, B), the slope was not significantly different from 1 ($p > 0.05$) and the intercept was not significantly different from 0 ($p > 0.05$).

Figure 5 shows the scatter plots of measured g_{st} versus each of the model input variables: PAR, T_{air}, VPD, and SWP, and for each plot the fitted boundary function.

The average daily O_3 fluxes for the different years are presented in Fig. S2. Daily F_{st} ranges from ~~1.42~~ 1.12 to ~~2.00~~ 1.52 nmol O_3 m^{-2} day^{-1}. In 2011 the daily F_{st} was the lowest, while the highest values were observed in 2002. The annual average ratio F_{st}/F_{tot} varied between 24-28 % (Fig. S2). We observed the lowest ratios in the beginning and at the end of the growing season. Above-average ratios were observed at the peak of the growing season.

3.3 Ozone effects on GPP

~~Total GPP (mol C m^{-2} day^{-1}) was calculated for days with low stomatal O_3 uptake, high stomatal O_3 uptake and for the entire growing season, using both the EC-derived GPP data and the modelled GPP data (Table 3). For days with low stomatal O_3 uptake, the average daily total GPP was 0.48 mol C m-2 day-1, and the models reproduced GPP very well (Table 3). When we calculated total GPP for days with high stomatal O_3 uptake, the EC-derived fluxes were much higher than for the days with low stomatal O_3 uptake. This was probably due to the higher irradiation that typically occurs during high O_3 events and stimulates GPP. The higher GPP, however, also suggests that negative O_3 effects on GPP were highly unlikely. This is exacerbated by the fact that our models almost consistently underestimate GPP during high O_3 events (Table 3), whereas we hypothesised the exact opposite, namely that the models would overestimate GPP during these events because they were parameterised for low O_3 days. We also observed no differences between both models, suggesting no lagged O_3 effects on GPP (Table 3).~~

~~A weak, negative correlation between total GPP residuals and F_{st} exists for the GPP model trained without days with high stomatal O_3 uptake (Fig. 7, A), while a small positive correlation is shown for the GPP model which tested for lag effects of O_3 (Fig. 7, B). However, these differences were not statistically significant at $p<0.05$. For both models, correlations between total GPP residuals and AOT40, and between total GPP residuals and both POD_1 and POD_2 existed. These correlations were also not statistically significant at $p<0.05$ (Fig. 7, C, D, E, F, G, and H).~~

Figure 6 shows the frequency distributions of R_g, T_{min}, T_{max}, T_{mean}, and VPD for the training dataset and the dataset with days on which we assumed an O_3 effect. Days in the latter dataset are generally more concentrated in the upper half of each variable's range. The training dataset includes more days in the lower half, but conditions of high radiation, temperature or VPD do not seem to be underrepresented as the dataset also included a substantial number of days in the higher part. For all variables, the variable range of the dataset with days for we assumed an O_3 effect is fully contained range of the training dataset.

To test for carry-over O_3 effects, we evaluated and compared the linear regressions of measured versus modelled GPP of a dataset with low O_3 fluxes after the first major O_3 flux peak in the growing season and a dataset before this peak (Fig. 7). For both regressions, intercept and slope were not significantly different from 0 and 1 respectively (training: $p_{slope} = 1$, $p_{intercept} = 1$, testing: $p_{slope} = 0.83$, $p_{intercept} = 0.44$). The slopes were also not significantly different from each other ($p = 0.86$) and neither were the intercepts ($p = 0.53$).

Figure 8 shows measured versus modelled daily GPP for the model trained without the days with the highest stomatal O_3 fluxes (GPP model 1) and the model trained to test also for lag effects (GPP model 2). Both models reproduced daily GPP well for the dataset against which they were trained and tested, as indicated by the high R^2 values and the fitted regression lines falling on the 1:1 line (Fig. 8 A, B). For both models, the regression slope for the dataset with the days on which we assumed an O_3 effect was significantly lower than 1 and the intercept significantly higher than 0 (Fig. 8 C, D). For GPP model 1, the regression slopes were not significantly different between the two datasets ($p = 0.46$), but the intercepts were ($p < 0.05$). For GPP model 2, both the regression slopes and intercepts differed significantly ($p < 0.001$) and $p < 0.001$). However, a Wilcoxon signed-rank test showed for both models that modelled daily GPP was not significantly higher than measured daily GPP for the days on which an O_3 effect was assumed ($p = 0.83$ and $p = 0.64$, respectively). Also, a paired samples t-test showed for both models that modelled growing season GPP was not significantly higher than measured growing season GPP ($p = 0.93$ and $p = 0.55$, respectively). The slope and intercept of the linear regression line were not significantly different from 1 and 0 (Fig. 8 e, f).

No statistically significant correlations were found between the model residuals of growing season GPP and total stomatal O_3 uptake (F_{st}), AOT40, and POD_1 (Fig. 9).

4 Discussion

4.1 Multiplicative stomatal model

All statistics shown in Table 2 clearly indicated that the fitted multiplicative stomatal model performed well. For both parameterisation and validation datasets, the model explained 72 % of the variance in g_{st}. For both datasets, slope and intercept of the linear regression lines of measured versus modelled g_{st} were not significantly different from 1 and 0, respectively (Fig. 4). Moreover, the model efficiency (ME in Table 2) of 0.72 and the Wilmott's index (d) close to 1 both indicate that the modelled values matched the measured values well. A good model provides low root-mean-square error (RMSE), while the systematic component ($RMSE_s$) should approach zero and the unsystematic component ($RMSE_u$) should approach RMSE (Willmott et al., 1985), which was the case for this model. Low mean bias (MB) and low mean relative error (MRE) further indicated very good performance. The good performance of the model can also be observed in Fig. 5, in which the boundary lines represented the response of g_{st} to the independent variables when other variables were not limiting (Martin et al., 1997). The boundary lines fitted close to the data points, which is an indication of a good model, because the multiplicative stomatal model is based on the assumption that the variables act more or less multiplicatively and independently from each other (Grüters et al., 1995).

Multiplicative stomatal models based on Jarvis (1976) have been parameterised earlier for generic Scots pine forests in Europe (Mills et al., 2011;Buker et al., 2015) and used to estimate critical levels for this species. However, the empirical dose-response relationship for Scots pine is based on only one two-year fumigation study on small seedlings and, therefore, high uncertainty exists in the modelled O_3 impact on Scots pine growth.

The parameterisation of Mills et al. (2011) and Büker et al. (2015) differ from that of this study in a number of parameters. First, the needles of the Scots pine stand in Brasschaat had a higher night-time g_{st} (g_{min}) and will therefore take up more O_3 at night. Maximal g_{st}, in contrast, is lower in Brasschaat than estimated for other Scots pine forests, implying that during episodes of high O_3 mixing ratio, the Brasschaat site is unlikely to take up very high amounts of O_3. This may have contributed to the absence of a clear O_3 response at our study site. Also the Scots pine stand in Brasschaat is less sensitive to drought stress than the generic model, due to a higher VPD_{max} and a wider SWP range. The wider SWP range is mainly due to a clearly lower SWP_{max}. These differences between the parameter values and, hence, in g_{st} for generic Scots pine forests and for the Scots pine stand in Brasschaat will lead to different critical levels and under- or overestimation of possible O_3 damage. Species-specific parameterisation is important, but site-specific parameterisation is clearly important as well.

4.2 Stomatal O_3 fluxes

The stomatal O_3 flux contributed on average for 26 % to the total O_3 flux over the study period (Fig. S2). This fraction is similar to the 21 % stomatal O_3 flux in a Danish Norway spruce stand (Mikkelsen et al., 2004) and the 30 % stomatal O_3 flux in *Quercus ilex* in Italy (Vitale et al., 2005;Gerosa et al., 2005). Cieslik (2004) showed that in Southern Europe stomatal O_3 flux of different vegetation types, such as pine forest and Mediterranean shrubs, is typically less than 50 % of the total O_3 flux. A five-year study on a Mediterranean *Pinus ponderosa* stand showed a stomatal O_3 flux contribution of 57 % (Fares et al., 2010). Clearly, species- and site-specific differences such as tree age or micro-climate are introducing large variability in stomatal O_3 uptake (Neirynck et al., 2012).

The low relative stomatal O_3 flux in the Scots pine stand in Brasschaat could be the result of the sparse canopy with low LAI. Although no relation between stomatal O_3 flux and LAI was found in a previous site study on this site (Neirynck et al., 2012), interannual and seasonal variation in LAI is very small, rendering such a correlation analysis very difficult.

4.3 Ozone effects on GPP

A comparison of the frequency distributions of radiation, temperature, and VPD between the training dataset and the dataset with the days on which we expected an O_3 effect showed that the meteorological conditions in the latter dataset were fully represented in the training dataset. From the full overlap we can rather safely assume that the GPP model did not to include a biased response to these variables that could result in a GPP overestimation that we might wrongly interpret as an effect of O_3. Also, a GPP model parameterized to include a carry-over effect of O_3 on GPP did not overestimate GPP at a statistically detectable level for days on which such an effect was not assumed to occur. From these results, we infer that carry-over effects of O_3 were unlikely to have occurred and that the assumption on the absence of (detectable) carry-over effects was valid.

The statistical tests ran on the datasets of measured and modelled GPP did not reveal a statistically significant model overestimation of daily GPP for the days on which we assumed an O_3 effect, nor an overestimation of growing season GPP. Also no significant correlations between growing season GPP residuals and stomatal O_3 flux, AOT40, and POD_1 were found, even though critical levels for AOT40 and POD_1 were exceeded in every single year of our study period. From these results and within the limits of the modelling approach applied in this study, we can infer that no significant effect of O_3 on GPP occurred.

~~Although our models reproduced GPP very well, we did not observe immediate or lagged effects of high stomatal O3 uptake on GPP (Table 3; Fig. 7, A, B).~~ Some earlier studies have investigated the effect of O_3 on forest carbon uptake. Cumulative stomatal uptake of 27 mmol m^{-2} over the growing season did not result in any visible damage or a reduction in NEE of a poplar plantation in Belgium (Zona et al., 2014). Zapletal (2011), on the other hand, reported that CO_2 uptake of a Norway spruce forest in the Czech Republic increased with increasing stomatal O_3 flux, followed by a sudden decrease in CO_2 uptake, suggesting that an O_3 flux threshold exists. Fares (2013) showed a negative correlation between GPP and O_3 uptake at two Mediterranean ecosystems (a forest dominated by *Pinus ponderosa* in California, USA and an orchard site of *Citrus sinensis* cultivated in California, USA). A GPP reduction of 1-16% in response to O_3 uptake under ambient O_3 mixing ratio of 30-50 ppb was determined across vegetation types and environmental conditions in the United States by Yue and Unger (2013). The magnitude of reduction depended on the sensitivity to O_3 of the species and on the biome types.

AOT40 is, at present, the European standard for forest protection (EEA, 2014), with a critical level of 5000 ppb h, equivalent to a growth reduction of 5 % (Mills et al., 2011). In this study on Scots pine in Brasschaat, this value was far exceeded in all years (Fig. 9), yet no negative effect on GPP was observed in years with higher AOT40 values. ~~Particularly noteworthy is the extreme high AOT40 value of 2006, which was due to the high O3 concentration during that year, which, nevertheless, did not result in GPP reductions (Table 3).~~

POD~~y~~$_1$ is considered a more appropriate index for potential O_3 damage because it considers O_3 flux. The critical level of POD_1 is species-specific; a critical level of 8 mmol m^{-2} with 2 % growth reduction is used for Norway spruce and a critical level of 4 mmol m^{-2} with 4 % growth reduction is used for birch and beech (Mills et al., 2011). A critical level for Scots pine has not yet been determined and therefore the value of 8 mmol m^{-2} for Norway spruce is often adopted as critical level for Scots pine. During this study, this critical level was exceeded every single year, and again no significantly negative correlation between total GPP residuals and POD_1 was observed. In comparison to the AOT40 level, 2006 was not the year with the highest POD_1. This difference between AOT40 and POD_1 during 2006 was due to stomatal closure; during high O_3 mixing ratio events, g_{st} was rather low (~~Fig. 6~~Fig. S3). POD_1 was highest in the year 2002, when O_3 mixing ratios were relatively low, but g_{st} was high. The low O_3 mixing ratios explain the lower AOT40 for 2002.

Notwithstanding the absence of a statistically significant positive correlation between GPP residuals and both AOT40 and POD_1, critical levels for both AOT40 and POD_1 were exceeded every single year. AOT40 is based on O_3 mixing ratio and these concentration-based indices have been shown to be weaker indicators for O_3 damage than flux-based indices (Karlsson et al., 2007;Simpson et al., 2007). The critical level of POD_1 for Scots pine was adopted from the critical level for Norway spruce (Mills et al., 2011). Possibly this critical level is too low for

Scots pine. As shown by Reich (1987), pines are less sensitive to O_3 compared to hardwoods and crops. This supports the idea of a too low critical level.

Overall, no significant O_3 effects on GPP accumulated over the growing season were found. Although no significant O_3 effects on GPP were found in this study, it is still possible that O_3 negatively affected this Scots pine stand in Brasschaat. Stomatal O_3 uptake was linked to reductions in GPP only. As already stated in the introduction, protective responses such as compensation and enhanced tolerance occur in trees (Skärby et al., 1998). It is likely that trees at our study site were able to fully detoxify the incorporated O_3. As a result, no O_3 effects on carbon uptake were detectable. However, this protection may have come at a respiratory cost, which may have reduced the NPP/GPP ratio of this forest. The NPP/GPP ratio of our study site was very low (Gielen et al., 2013). In addition to the poor nutrient status (limitation by P and Mg, extremely high N deposition; (Neirynck et al., 2008)), O_3 uptake may partly be responsible. This can, however, not be tested because pine forest NPP data were not available at annual timescale.

5 Summary

We parameterised a multiplicative stomatal model for a Scots pine stand in Brasschaat. This species- and site-specific parameterised model performed very well. With this model embedded in a resistance scheme, stomatal O_3 fluxes were calculated and used to test for O_3 effects on GPP. Only very small reductions in growing season GPP were calculated. Although critical levels for AOT40 and POD~~y~~$_1$ were exceeded in every single year, no significant correlations between total GPP residuals and stomatal O_3 flux, AOT40, and POD~~y~~$_1$ were found. In general, we can thus conclude that no O_3 effects were detected on the carbon uptake by the Scots pine stand in Brasschaat.

Appendix A The multiplicative stomatal model

In this work the multiplicative stomatal model described by Jarvis (1976) is modified specificly for the Scots pine stand in Brasschaat. The basic model is explained below.

~~The multiplicative stomatal model is described by Jarvis (1976) and modified by Emberson (2000);~~ Stomatal conductance to O_3 at needle level (g_{st}) was modelled with the multiplicative stomatal model first described by Jarvis (1976) and later reformulated by (Emberson et al., 2000). In this study we used a modified version of the model (Eq. 1).

$$g_{st} = g_{max} * f_{phen} * (f_{min} + (1 - f_{min}) * (f_{PAR} * f_T * f_{VPD} * f_{SWP})) \qquad \text{(A1)}$$

~~where~~Here g_{st} is the stomatal conductance to O_3 and g_{max} is the ~~species-specific~~ maximal stomatal conductance to O_3. ~~The other parameters are expressed in relative terms as a proportion of g_{max}; f_{min} is the ratio of g_{min} to g_{max}; where g_{min} is the minimal stomatal conductance that occurs during daylight period; fphen represents the modification of g_{max} due to phenological changes; fPAR represents the modification of gmax by photosynthetically active radiation (PAR); fT represents the modification of gmax by air temperature (T_{air}); fVPD represents the modification of g_{max} by vapour pressure deficit (VPD); fSWP represents the modification of g_{max} by soil water potential (SWP).~~ The functions fPHEN, fPAR, fT, fVPD, and fSWP represent the modification of g_{max} by, respectively, phenology, PAR, T_{air}, VPD, and SWP. The function f_{min} is the ratio of g_{min} and g_{max} where g_{min} is the minimal stomatal conductance to O_3. Impaired stomatal aperture mechanisms (stomatal sluggishness) due to O_3 exposure (Paoletti and Grulke, 2010) were not included in this model. In this modified version PAR, T_{air}, VPD, and SWP influence the range between g_{max} and g_{min} instead of g_{max} and zero. This modification was needed, to allow modelling the observed non-zero g_{st} during nighttime (Op de Beeck et al., 2010).

Phenology modifies g_{max} because of the variation in g_{st} due to differences in needle age. The function f_{PHEN} is modelled as follows: (A2)

if $SGS \le doy \le (SGS + c)$, then $f_{PHEN} = f_{min} + (1 - f_{min}) * (1 - b) * \left(\frac{doy - SGS}{c}\right) + b$

if $SGS + c \le doy \le EGS - d$, then $f_{PHEN} = f_{min} + (1 - f_{min}) * 1$

if $EGS - d \le doy \le EGS$, then $f_{PHEN} = f_{min} + (1 - f_{min}) * (1 - b) * \left(\frac{EGS - doy}{d}\right) + b$

where SGS is the start of the growing season (doy = 115), EGS is the end of the growing season (doy = 300), and b (= 0.8) , c (= 20) , and d (= 20) are species-specific parameters representing the minimum of f_{PHEN}, the number of days for f_{PHEN} to reach its maximum and the number of days during the decline of f_{PHEN} for the minimum to reach again, assuming linear increase and decrease at the start and end of the growing season.

The stomatal response to PAR is described by a rectangular hyperbola, where a_{PAR} is a species-specific parameter determining the shape of the hyperbola (Emberson et al., 2000);

$$f_{PAR} = 1 - \exp(-a_{PAR} * PAR) \quad \text{(A3)}$$

The stomatal response to T_{air} is given by a parabolic function, where T_{min} is the minimum temperature at which stomatal opening occurs, and T_{opt} is the optimum temperature of stomatal opening (Emberson et al., 2000);

$$f_T = \max(0; 1 - \frac{(T - T_{opt})^2}{(T_{opt} - T_{min})^2}) \quad \text{(A4)}$$

The stomatal response to VPD is described by the following relationship, where VPD_{min} is a threshold for minimal stomatal opening, and VPD_{max} is a threshold for full stomatal opening (Emberson et al., 2000);

$$f_{VPD} = \min(1; \max\left(0; \frac{VPD_{min} - VPD}{VPD_{min} - VPD_{max}}\right)) \quad \text{(A5)}$$

The stomatal response to SWP is described by the following relationship, where SWP_{min} is a threshold for minimal stomatal opening, and SWP_{max} is a threshold for full stomatal opening (Emberson et al., 2000);

$$f_{SWP} = \min(1; \max\left(0; \frac{SWP_{min} - SWP}{SWP_{min} - SWP_{max}}\right)) \quad \text{(A6)}$$

Appendix B Statistics of model performance

In order to test how well the modified stomatal model performed, several model statistics were calculated. These model statistics are explained below.

The mean bias (MB) is the mean difference between the simulations (S_i) and the observations (O_i), with n being the number of data points (Stone, 1993);

$$MB = n^{-1} \sum_{i=1}^{n} (S_i - O_i) \quad \text{(B1)}$$

The mean relative error (MRE) is the mean relative difference between the simulations and the observations (Peierls, 1935);

$$MRE = n^{-1} \sum_{i=1}^{n} \frac{|S_i - O_i|}{O_i} \quad \text{(B2)}$$

Willmott's index of agreement (d) is a dimensionless goodness-of-fit coefficient, with $\bar{O}$ being the mean observation (Willmott, 1981); The index can vary between 0 and 1, with d equals 1 for a perfect agreement between simulations and observations.

$$d = 1 - \frac{\sum_{i=1}^{n} (S_i - O_i)^2}{\sum_{i=1}^{n} (|S_i - \bar{O}| + |O_i - \bar{O}|)} \quad \text{(B3)}$$

The model efficiency (ME) gives an indication of how well the observations match the simulations (Nash and Sutcliffe, 1970); Model efficiency can range from -∞ to 1 and is 1 when simulations and observations match perfectly. An efficiency of 0 indicates that the simulations are as accurate as the mean observation and an efficiency of less than zero indicates that the mean observation is a better predictor than the model.

$$ME = 1 - \frac{\sum_{i=1}^{n} (S_i - O_i)^2}{\sum_{i=1}^{n} (O_i - \bar{O})^2} \quad \text{(B4)}$$

The root-mean-squared error (RMSE) is a measure of the mean absolute difference between the simulations and the observations, weighting large differences heavily (Willmott et al., 1985); The systematic component ($RMSE_s$) estimates the model's linear or systematic error, hence, the better the regression between simulations and observations, the smaller the systematic component (Willmott et al., 1985). The unsystematic component is a measure of how much of the discrepancy between simulations and observations is due to random processes (Willmott et al., 1985). A good model will provide low values of RMSE, with $RMSE_s$ close to zero and $RMSE_u$ close to RMSE (Willmott et al., 1985).

$$RMSE = \sqrt{n^{-1} \sum_{i=1}^{n} (S_i - O_i)^2} \quad \text{(B5)}$$

$$RMSE_s = \sqrt{n^{-1} \sum_{i=1}^{n} ({S'}_i - O_i)^2} \quad \text{(B6)}$$

$$RMSE_u = \sqrt{n^{-1} \sum_{i=1}^{n} (S_i - {S'}_i)^2} \quad \text{(B7)}$$

$S'_i = a * O_i + b$, where ‘a’ and ‘b’ are slope and intercept, respectively, of the linear regression of the simulations versus the observations.

~~Appendix C The canopy model~~

~~*Stomatal conductance was calculated on leaf level with the stomatal model. The canopy model was used to scale up these values for the whole canopy. Ozone fluxes were calculated, based on an electrical conductance analogy. Below the general canopy model, including conductance analogy model, is explained, followed by the explanation of two submodel that were used: solar elevation submodel and radiation submodel.*~~

~~Part 1 The canopy model~~

~~The canopy model is an algorithm to scale up g_{st} at leaf level to g_{st} at canopy level. Subsequently, O_3 fluxes are calculated with an electrical conductance analogy model, which calculates the instant canopy O_3 uptake from different input data Rg, T_{air}, VPD, LAI, SWP, and O_3 mixing ratio. The canopy model consists of three submodels: the multiplicative stomatal model (Appendix A), the solar elevation submodel, and the radiation transfer submodel (see below).~~

~~First, the canopy is divided into different horizontal layers, with each a sunlit and shaded fraction. For each layer fraction the incoming PAR is calculated with the radiation transfer submodel. With the multiplicative stomatal model g_{st} is calculated for each layer fraction.~~

~~For each layer fraction the total leaf conductance (mol m^{-2} leaf area s^{-1}) is calculated by summing g_{st} and g_{ns}, the non-stomatal conductance. This value is multiplied by LAI of the layer fraction and the values for both the sunlit and the shaded layer fraction are summed to obtain the total layer conductance (mol m^{-2} ground area s^{-1}). All layer conductances can be summed to obtain the conductance of the canopy as a whole (g_{can}).~~

~~The total conductance is a function of g_{bl} and g_{can} based on an electrical conductance analogy model.~~

$$\cancel{g_{tot} = \left(\frac{1}{g_{aero}} + \frac{1}{g_{bl}} + \frac{1}{g_{can}}\right)^{-1} \qquad (C1)}$$

~~where g_{aero} is the aerodynamic conductance; g_{bl} is the boundary layer conductance; g_{can} is the canopy conductance.~~

$$\cancel{g_{aero} = \frac{1}{\kappa u^*}\left[\ln\left(\frac{z-d}{z_0}\right) - \Psi_h\left(\frac{z-d}{L}\right) + \Psi_h\left(\frac{z_0}{L}\right)\right] \qquad (C2)}$$

~~where the von Karman constant κ = 0.43; u* (m s-1) is the friction velocity; L is the obukov length; z is the height at which the O_3 mixing ratio was measured ;~~

~~where $z_{0m} = 0.1 * h$ and $d = 0.65 * h$ with h is the canopy height; and~~

~~where the atmospheric stratification function Ψ_h is calculated as:~~

- ~~Unstable atmospheric stratification (L < 0m):~~

  ~~$\Psi_h = 2 * \ln[\frac{1}{\varphi_h(\zeta)} + 1]$~~

  ~~with $\varphi_h = (1 - 16 * \zeta)^{-0.5}$~~

  ~~and $\zeta = \frac{z-d}{L}$ with $z = z_2 = z_{ref,I}$ and $z = z_1 = d + z_{0m}$ and L = the Obukov length~~
- ~~Stable atmospheric stratification (L > 0m):~~

  ~~$\Psi_h = -5 * \zeta$~~

  ~~with $\zeta = \frac{z-d}{L}$ with $z = z_2 = z_{ref,I}$ and $z = z_1 = d + z_{0m}$ and L = the Obukov length~~
- ~~Neutral atmospheric stratification (|L| → ∞):~~

  ~~$\Psi_h = 0$~~

~~Total O_3 flux (nmol m^{-2} ground area s^{-1}) is the O_3 flux for the whole canopy and is then calculated by:~~

~~$F_{tot} = [O_3] * g_{tot}$ (C3)~~

~~where $[O_3]$ is the O_3 mixing ratio (ppb).~~

~~Stomatal O_3 flux is the fraction of the total O_3 flux taken up by the stomata and is calculated by:~~

~~$F_{st} = F_{st} * \frac{g_{st}}{g_{st}+g_{ns}}$ (C4)~~

~~where g_{st} is the stomatal conductance (mol m^{-2} ground area s^{-1}); g_{ns} is the non-stomatal conductance (mol m^{-2} ground area s^{-1}).~~

~~Non-stomatal O_3 flux (F_{ns}) is the difference between total O_3 flux and stomatal O_3 flux:~~

~~$F_{ns} = F_{tot} - F_{st}$ (C5)~~

~~Part 2 The solar elevation submodel~~

~~This submodel calculates the solar elevation angle, β (radians), at each time step (Campbell and Norman, 1998).~~

~~$\beta = \arcsin(\sin\phi \sin\delta + \cos\phi \cos\delta \cos h)$ (C6)~~

~~where δ is the solar declination angle; $\delta = -23.4 * \left(\frac{\pi}{180}\right) * \cos(2 * \pi * \frac{doy+10}{365})$~~

~~ϕ is the latitude in radians; $\phi = 0.89$~~

~~h is the hour angle of the sun; $h = \pi * \frac{t-t_0}{12.0}$~~

~~where t is time; t_0 is solar noon; $t_0 = 12 + \frac{4*(L_s-L_l)-E_t}{60.0}$~~

~~L_s is the standard longitude in degrees; $L_s = 15.0$~~

~~L_l is the local longitude in degrees; $L_l = 4.0$~~

~~E_t is the empheris of the sun;~~

~~$$E_t = 0.017 + 0.4281 * \cos(F_d) - 7.351 * \sin(F_d) - 3.349 * \cos(2 * F_d) - 9.731 * \sin(F_d)$$~~

~~where F_d is the day angle; $F_d = 2 * \pi * \frac{doy-1}{365}$~~

~~**Part 3 The radiation transfer submodel**~~

~~The radiation submodel calculates the direct (I_{b0}) and diffuse (I_{d0}) fraction of the incoming radiation (I) at the top of the canopy. Hence, I is equal to R_g. These calculation is based on the difference between measured and theoretically potential incoming radiation above the canopy, which is depending on β, the solar elevation angle (Op de Beeck et al., 2010).~~

~~First the sunlit LAI fraction of each horizontal leaf layer i is calculated with Beer's law:~~

~~$$f_{sun(i)} = \exp(-k_b \Omega LAI_{c(i)}) \qquad (C7)$$~~

~~where k_b is the direct radiation extinction coefficient; Ω is a factor accounting for inter- and intra-crown foliage clumping; $LAI_{c(i)}$ is the cumulative LAI above a horizontal leaf layer i.~~

~~A spherical needle angle distribution is assumed, hence $k_b = 0.5/\sin\beta$ (de Pury, 1997).~~

~~The shaded LAI fraction of each horizontal leaf layer i is calculated as follows:~~

~~$$f_{shad(i)} = 1 - f_{sun(i)} \qquad (C8)$$~~

~~where fsun(i) is the sunlit LAI fraction.~~

~~The intensity of direct radiation does not decline through the canopy, but the diffuse radiation does and is calculated with Beer's law:~~

~~$I_{d(i)} = I_{d0} * \exp(k_d \Omega LAI_{c(i)})$ (C9)~~

~~where I_{d0} is the incoming diffuse radiation.~~

~~The total received radiation by a sunlit fraction ($I_{sun(i)}$) is the sum of direct and diffuse radiation. Shaded leaves only receive diffuse radiation:~~

~~$I_{shad(i)} = I_{d(i)}$ (C10)~~

~~$I_{sun(i)} = \cos\left(\frac{\pi}{3}\right) * I_{b0} + I_{d(i)}$ (C9)~~

~~where $\left(\frac{\pi}{3}\right)$ is the averaged leaf angle for a uniform needle angle distribution; I_{b0} is the incoming direct radiation at top of the canopy; $I_{d(i)}$ is the diffuse radiation for a horizontal leaf layer i.~~

~~Total received irradiance is now converted to total received PAR and split into PAR per horizontal leaf layer.~~

Author contribution L.T. Verryckt, M. Op de Beeck, B. Gielen, M. Roland and I.A. Janssens designed the study. J. Neirynck provided the O_3 mixing ratio measurements, B. Gielen provided the EC and LAI data, B. Gielen, M. Op de Beeck and L.T. Verryckt measured g_{st} in situ, and M. Op de Beeck and L.T. Verryckt conducted the modelling. All authors contributed to the writing.

Acknowledgement The measurements for this work were funded by the Hercules Foundation, through support of the Brasschaat ICOS ecosystem station. IAJ acknowledges support from the European Research Council Synergy grant ERC-2013-SyG-610028 IMBALANCE-P.

References

Andersen, C. P., Wilson, R., Plocher, M., and Hogsett, W. E.: Carry-over effects of ozone on root growth and carbohydrate concentrations of ponderosa pine seedlings, Tree Physiol., 17, 805-811, 1997.

Baldocchi, D. D., Hicks, B. B., and Camara, P.: A canopy stomatal resistance model for gaseous deposition to vegetated surfaces, Atmos. Environ., 21, 91-101, http://dx.doi.org/10.1016/0004-6981(87)90274-5, 1987.

Beedlow, P. A., Tingey, D. T., Phillips, D. L., Hogsett, W. E., and Olszyk, D. M.: Rising atmospheric CO2 and carbon sequestration in forests, Front. Ecol. Environ., 2, 315-322, 2004.

Buker, P., Feng, Z., Uddling, J., Briolat, A., Alonso, R., Braun, S., Elvira, S., Gerosa, G., Karlsson, P. E., Le Thiec, D., Marzuoli, R., Mills, G., Oksanen, E., Wieser, G., Wilkinson, M., and Emberson, L. D.: New flux based dose-response relationships for ozone for European forest tree species, Environ. Pollut., 206, 163-174, 10.1016/j.envpol.2015.06.033, 2015.

Carrara, A., Kowalski, A. S., Neirynck, J., Janssens, I. A., Yuste, J. C., and Ceulemans, R.: Net ecosystem CO2 exchange of mixed forest in Belgium over 5 years, Agr. Forest Meteorol., 119, 209-227, 10.1016/s0168-1923(03)00120-5, 2003.

Carrara, A., Janssens, I. A., Curiel Yuste, J., and Ceulemans, R.: Seasonal changes in photosynthesis, respiration and NEE of a mixed temperate forest, Agr. Forest Meteorol., 126, 15-31, 10.1016/j.agrformet.2004.05.002, 2004.

Chappelka, A. H., and Samuelson, L. J.: Ambient ozone effects on forest trees of eastern United States: a review, New Phytol., 139, 91-108, 1998.

Cieslik, S. A.: Ozone uptake by various surface types: a comparison between dose and exposure, Atmos. Environ., 38, 2409-2420, 10.1016/j.atmosenv.2003.10.063, 2004.

Darall, N. M.: The effect of air pollutants on physiological processes in plants, Plant Cell Environ., 12, 1-30, 1989.

Dyer, A. J.: A review of flux-profile relationships, Bound-Lay Meteorol., 7, 363-372, 10.1007/bf00240838, 1974.

European Environment Agency: http://www.eea.europa.eu/, access: 1 May, 2014.

Emberson, L. D., Ashmore, M. R., Cambridge, H. M., Simpson, D., and Tuovinen, J. P.: Modelling stomatal ozone flux across Europe, Environ. Pollut., 109, 403-413, 2000.

Falge, E., Baldocchi, D., Olson, R., Anthoni, P., Aubinet, M., Bernhofer, C., Burba, G., Ceulemans, R., Clement, R., Dolman, H., Granier, A., Gross, P., Grünwald, T., Hollinger, D., Jensen, N.-O., Katul, G., Keronen, P., Kowalski, A., Ta Lai, C., Law, B. E., Meyers, T., Moncrieff, J., Moors, E., Munger, J. W., Pilegaard, K., Rannick, Ü., Rebmann, C., Suyker, A., Tenhunen, J., Tu, K., Verma, S., Vesala, T., Wilson, K., and Wofsy, S.: Gap filling strategies for long term energy flux data sets, Agr. Forest Meteorol., 107, 71-77, 2001.

Fares, S., McKay, M., Holzinger, R., and Goldstein, A. H.: Ozone fluxes in a Pinus ponderosa ecosystem are dominated by non-stomatal processes: Evidence from long-term continuous measurements, Agr. Forest Meteorol., 150, 420-431, http://dx.doi.org/10.1016/j.agrformet.2010.01.007, 2010.

Fares, S., Vargas, R., Detto, M., Goldstein, A. H., Karlik, J., Paoletti, E., and Vitale, M.: Tropospheric ozone reduces carbon assimilation in trees: estimates from analysis of continuous flux measurements, Glob. Change Biol., 19, 2427-2443, 10.1111/gcb.12222, 2013.

Gerosa, G., Vitale, M., Finco, A., Manes, F., Denti, A., and Cieslik, S.: Ozone uptake by an evergreen Mediterranean Forest () in Italy. Part I: Micrometeorological flux measurements and flux partitioning, Atmos. Environ., 39, 3255-3266, 10.1016/j.atmosenv.2005.01.056, 2005.

Gielen, B., Verbeeck, H., Neirynck, J., Sampson, D. A., Vermeiren, F., and Janssens, I. A.: Decadal water balance of a temperate Scots pine forest (Pinus sylvestris L.) based on measurements and modelling, Biogeosciences, 7, 1247-1261, 2010.

Gielen, B., Neirynck, J., Luyssaert, S., and Janssens, I. A.: The importance of dissolved organic carbon fluxes for the carbon balance of a temperate Scots pine forest, Agr. Forest Meteorol., 151, 270-278, 10.1016/j.agrformet.2010.10.012, 2011.

Gielen, B., De Vos, B., Campioli, M., Neirynck, J., Papale, D., Verstraeten, A., Ceulemans, R., and Janssens, I. A.: Biometric and eddy covariance-based assessment of decadal carbon sequestration of a temperate Scots pine forest, Agr. Forest Meteorol., 174-175, 135-143, 10.1016/j.agrformet.2013.02.008, 2013.

Gond, V., De Pury, D. G. G., Veroustraete, F., and Ceulemans, R.: Seasonal variations in leaf area index, leaf chlorophyll, and water content; scaling-up to estimate fAPAR and carbon balance in a multilayer, multispecies temperate forest, Tree Physiol., 19, 673-679, 1999.

Grünhage, L.: An O3 flux-based risk assessment for spring wheat., Joint ICP Vegetation/EMEP. Ad-hoc Expert Panel Meeting on Modelling and Mapping of Ozone Flux and Deposition to Vegetation to be held under the UN/ECE Convention on Long-range Transboundary Air Pollution, 2002.

Grüters, U., Fangmeier, A., and Jäger, H.-J.: Modelling stomatal responses of spring wheat (Triticum aestivum L. cv. Turbo) to ozone and different levels of water supply, Environ. Pollut., 87, 141-149, 1995.

ICP Vegetation: Yield response and ozone injury on Phaseolus vulgaris. Experimental Protocol., 2012.

Climate Change 2001: Impacts, Adaptation, and Vulnerability. A report of working group I of the Intergovernmental Panel on Climate Change.: http://www.ipcc.ch/, 2001.

IPCC: Climate Change 2007: Synthesis Report. Contribution to Working Group I, II and III to the Fourth Assessment Report of the Intergovernmental Panel on Climate Change., Geneva, Switzerland, 104, 2007.

Janssens, I. A., Sampson, D. A., Cermak, J., Meiresonne, L., Riguzzi, F., Overloop, S., and Ceuelemans, R.: Above- and belowground pyhtomass and carbon storage in a Belgian Scots pine stand, Ann. For. Sci., 56, 81-90, 1999.

Jarvis, P. G.: The interpretation of the variations in leaf water potential and stomatal conductance found in canopies in the field, Philos. T. Roy. Soc. B., 273, 593-610, 1976.

Jonckheere, I., Muys, B., and Coppin, P.: Allometry and evaluation of in situ optical LAI determination in Scots pine: a case study in Belgium, Tree Physiol., 25, 2005.

Karlsson, P. E., Uddling, J., Braun, S., Broadmeadow, M., Elvira, S., Gimeno, B. S., Le Thiec, D., Oksanen, E., Vandermeiren, K., Wilkinson, M., and Emberson, L.: New critical levels for ozone effects on young trees based on AOT40 and simulated cumulative leaf uptake of ozone, Atmos. Environ., 38, 2283-2294, 10.1016/j.atmosenv.2004.01.027, 2004.

Karlsson, P. E., Braun, S., Broadmeadow, M., Elvira, S., Emberson, L., Gimeno, B. S., Le Thiec, D., Novak, K., Oksanen, E., Schaub, M., Uddling, J., and Wilkinson, M.: Risk assessments for forest trees: the performance of the ozone flux versus the AOT concepts, Environ. Pollut., 146, 608-616, 10.1016/j.envpol.2006.06.012, 2007.

Konôpka, B., Yuste, J. C., Janssens, I. A., and Ceulemans, R.: Comparison of Fine Root Dynamics in Scots Pine and Pedunculate Oak in Sandy Soil, Plant Soil, 276, 33-45, 10.1007/s11104-004-2976-3, 2005.

Martin, T. A., Brown, K. J., Carmák, J., Ceulemans, R., Kucera, J., Meinzer, F. C., Rombold, J. S., Sprugel, D. G., and Hinckley, T. M.: Crown conductance and tree and stand transpiration in a second growth Abies amibilis forest, Can. J. Forest Res., 27, 797-808, 1997.

Mauzerall, D. L., and Wang, X.: Protecting agricultural crops from the effects of tropospheric ozone exposure: Reconciling Science and Standard Setting in the United States, Europe, and Asia, Annu. Rev. Energy Env., 26, 237-268, doi:10.1146/annurev.energy.26.1.237, 2001.

McLaughlin, S. B., Nosal, M., Wullschleger, S. D., and Sun, G.: Interactive effects of ozone and climate on tree growth and water use in a southern Appalachian forest in the USA, New Phytol., 174, 109-124, 10.1111/j.1469-8137.2007.02018.x, 2007.

Middleton, J. T.: Response of Plants to Air Pollution, Journal of the Air Pollution Control Association, 6, 7-9, 10.1080/00966665.1956.10467730, 1956.

Mikkelsen, T. N., Ro-Poulsen, H., Hovmand, M. F., Jensen, N. O., Pilegaard, K., and Egeløv, A. H.: Five-year measurements of ozone fluxes to a Danish Norway spruce canopy, Atmos. Environ., 38, 2361-2371, http://dx.doi.org/10.1016/j.atmosenv.2003.12.036, 2004.

Musselman, R. C., and Massman, W. J.: Ozone flux to vegetation and its relationship to plant response and ambient air quality standards, Atmos. Environ., 33, 65-73, 1999.

Nash, J. E., and Sutcliffe, J. V.: River flow forecasting through conceptual models, J. Hydrol., 10, 282-290, 1970.

Neirynck, J., Janssens, I. A., Roskams, P., Quataert, P., Verschelde, P., and Ceulemans, R.: Nitrogen biogeochemistry of a mature Scots pine forest subjected to high nitrogen loads, Biogeochemistry, 91, 201-222, 10.1007/s10533-008-9280-x, 2008.

Neirynck, J., Gielen, B., Janssens, I. A., and Ceulemans, R.: Insights into ozone deposition patterns from decade-long ozone flux measurements over a mixed temperate forest, J. Environ. Monit., 14, 2012.

Noble, R. D., and Jensen, K. F.: Effects of sulfur dioxide and ozone on growth of hybrid poplar leaves, Am. J. Bot., 67, 1005-1009, 1980.

Op de Beeck, M., Gielen, B., Jonckheere, I., Samson, R., Janssens, I. A., and Ceulemans, R.: Needle age-related and seasonal photosynthetic capacity variation is negligible for modelling yearly gas exchange of a sparse temperate Scots pine forest, Biogeosciences, 7, 199-215, 2010.

Paoletti, E., and Grulke, N. E.: Ozone exposure and stomatal sluggishness in different plant physiognomic classes, Environ. Pollut., 158, 2664-2671, 10.1016/j.envpol.2010.04.024, 2010.

Peierls, R.: Statistical Error in Counting Experiments, P. Roy. Soc. A-Math Phy., 149, 467-486, 10.1098/rspa.1935.0076, 1935.

Reich, P. B., and Amundson, R. G.: Ambient levels of ozone reduce net photosynthesis in tree and crop species, Science, 230, 566-570, 1985.

Reich, P. B.: Quantifying plant response to ozone - a unifying theory, Tree Physiol., 3, 63-91, 1987.

Samuelson, L. J.: Ozone-exposure responses of Black-Cherry and Red Maple seedlings, Environ. Exp. Bot., 34, 355-362, 10.1016/0098-8472(94)90017-5, 1994.

Simpson, D., Ashmore, M. R., Emberson, L., and Tuovinen, J. P.: A comparison of two different approaches for mapping potential ozone damage to vegetation. A model study, Environ. Pollut., 146, 715-725, 10.1016/j.envpol.2006.04.013, 2007.

Skärby, L., Troeng, E., and Boström, C. A.: Ozone uptake and effects on transpiration, net photosynthesis and dark respiration in Scots pine, For. Sci., 33, 801-808, 1987.

Skärby, L., Ro-Poulsen, H., Wellburn, F. A. M., and Sheppard, L. J.: Impacts of ozone on forests: a European perspective, New Phytol., 139, 109-122, 1998.

Stone, R. J.: Improved statistical procedure for the evaluation of solar radiation estimation models, Solar Energy, 51, 289-291, 1993.

van Genuchten, M. T.: A Closed-form Equation for Predicting the Hydraulic Conductivity of Unsaturated Soils, 44, 892-898, 10.2136/sssaj1980.03615995004400050002x, 1980.

Vitale, M., Gerosa, G., Ballarindenti, A., and Manes, F.: Ozone uptake by an evergreen mediterranean forest (L.) in Italy—Part II: flux modelling. Upscaling leaf to canopy ozone uptake by a process-based model, Atmos. Environ., 39, 3267-3278, 10.1016/j.atmosenv.2005.01.057, 2005.

Willmott, C. J.: On the validation of models, Physical Geography, 2, 184-194, 1981.

Willmott, C. J., Ackleson, S. G., Davis, R. E., Feddema, J. J., Klink, K. M., Legates, D. R., O'Donnell, J., and Rowe, C. M.: Statistics for the evaluation and comparison of models, J. Geophys. Res., 90, 8995-9005, 1985.

Yue, X., and Unger, N.: Ozone vegetation damage effects on gross primary productivity in the United States, Atmos. Chem. Phys. Discussions, 13, 31563-31605, 10.5194/acpd-13-31563-2013, 2013.

Yuste, J. C., Konôpka, B., Janssens, I. A., Coenen, K., Xiao, C. W., and Ceulemans, R.: Contrasting net primary productivity and carbon distribution between neighboring stands of Quercus robur and Pinus sylvestris, Tree Physiol., 25, 701-712, 2005.

Zapletal, M., Cudlin, P., Chroust, P., Urban, O., Pokorny, R., Edwards-Jonasova, M., Czerny, R., Janous, D., Taufarova, K., Vecera, Z., Mikuska, P., and Paoletti, E.: Ozone flux over a Norway spruce forest and correlation with net ecosystem production, Environ. Pollut., 159, 1024-1034, 10.1016/j.envpol.2010.11.037, 2011.

Zona, D., Gioli, B., Fares, S., De Groote, T., Pilegaard, K., Ibrom, A., and Ceulemans, R.: Environmental controls on ozone fluxes in a poplar plantation in Western Europe, Environ. Pollut., 184, 201-210, 10.1016/j.envpol.2013.08.032, 2014.

Table 1. Optimised parameter values of the multiplicative stomatal model.

g_{min} (mol O_3 m^{-2} s^{-1})	0.02
g_{max} (mol O_3 m^{-2} s^{-1})	0.14
a	0.0057
T_{opt} (°C)	25.61
T_{min} (°C)	5.47
VPD_{min} (kPa)	3.16
VPD_{max} (kPa)	0.51
SWP_{min} (MPa)	-1.18
SWP_{max} (MPa)	-0.19

875 Table 2. Performance statistics for the multiplicative stomatal model: mean bias (MB), relative mean error (RME), systematic and unsystematic root mean squared error ($RMSE_{s/u}$), Willmott's index of agreement (d), model efficiency (ME), coefficient of determination (R^2).

Statistics	**Parameterisation**	**Validation**
MB	0.002	0.002
RME	0.34	0.33
RMSE	0.019	0.019
$RMSE_s$	0.006	0.006
$RMSE_u$	0.017	0.017
d	0.99	0.99
ME	0.72	0.72
R^2	0.72	0.72

Fig. 1. Fingerprint of air temperature (T_{air}), incoming global radiation (R_g), vapour pressure deficit (VPD), and measured gross primary productivity (GPP), averaged over the period 1998-2013. Day of year is plotted on the y-axis and hour of day on the x-axis.

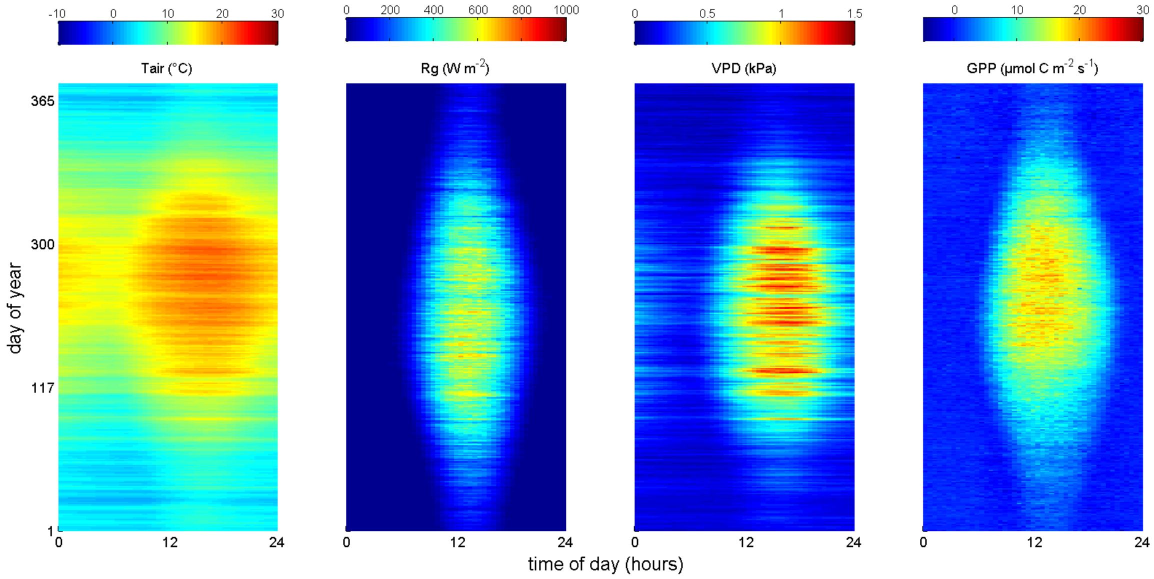

885 Fig. 2.Time series of the weekly total precipitation and mean soil water potential (SWP). The precipitation and SWP data are averaged over the period 1998-2013. Error bars represent the 95% confidence intervals.

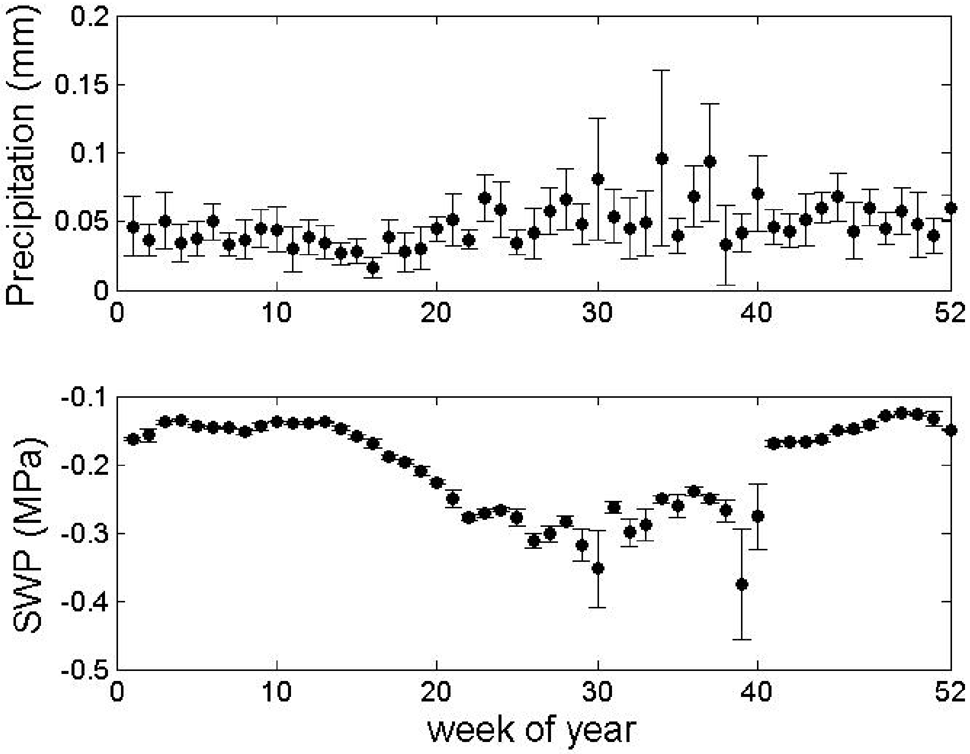

Fig. 3. Seasonal course of LAI for each of the 14 growing seasons used in this study.

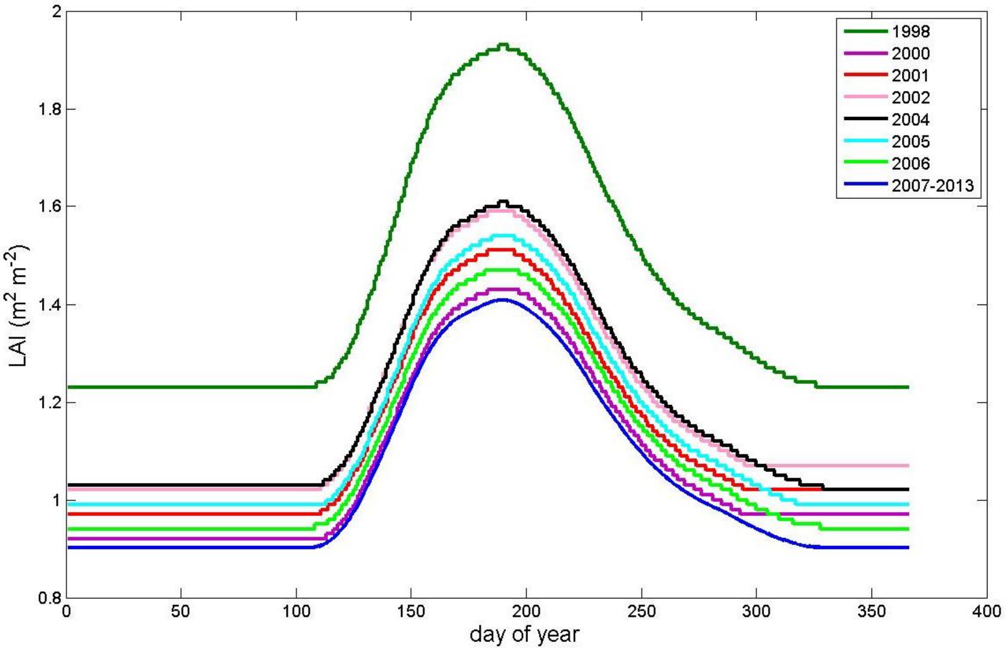

890

Fig. 4. Measured versus modelled stomatal conductance (g_{st}) for the parameterisation dataset (A) (n = 205) and the validation dataset (B) (n = 205). The black line is the 1:1 line. The red line is the linear fit for which the equation is given in the figure. Also shown are the p-values of test for the slope being different from 1 (p_a) and the intercept different from 0 (p_b).

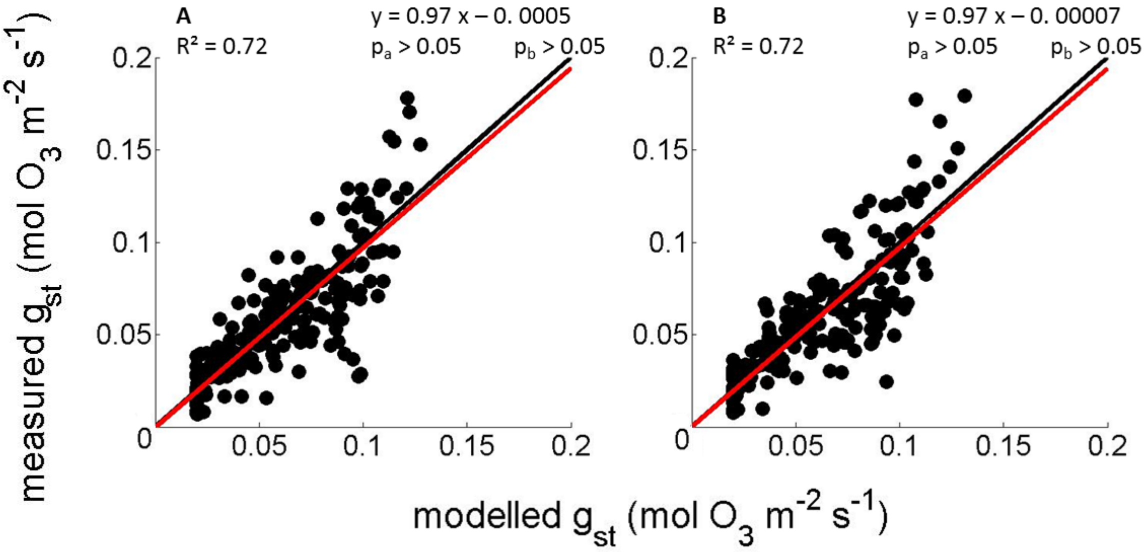

Fig. 5. Measured stomatal conductance (g_{st}) in function of the different variables used in the multiplicative model: photosynthetically active radiation (PAR), air temperature (T_{air}), vapour pressure deficit (VPD), and soil water potential (SWP). The red line represents the boundary line for which the functions are given in Appendix A (A3-A6). (n = 205)

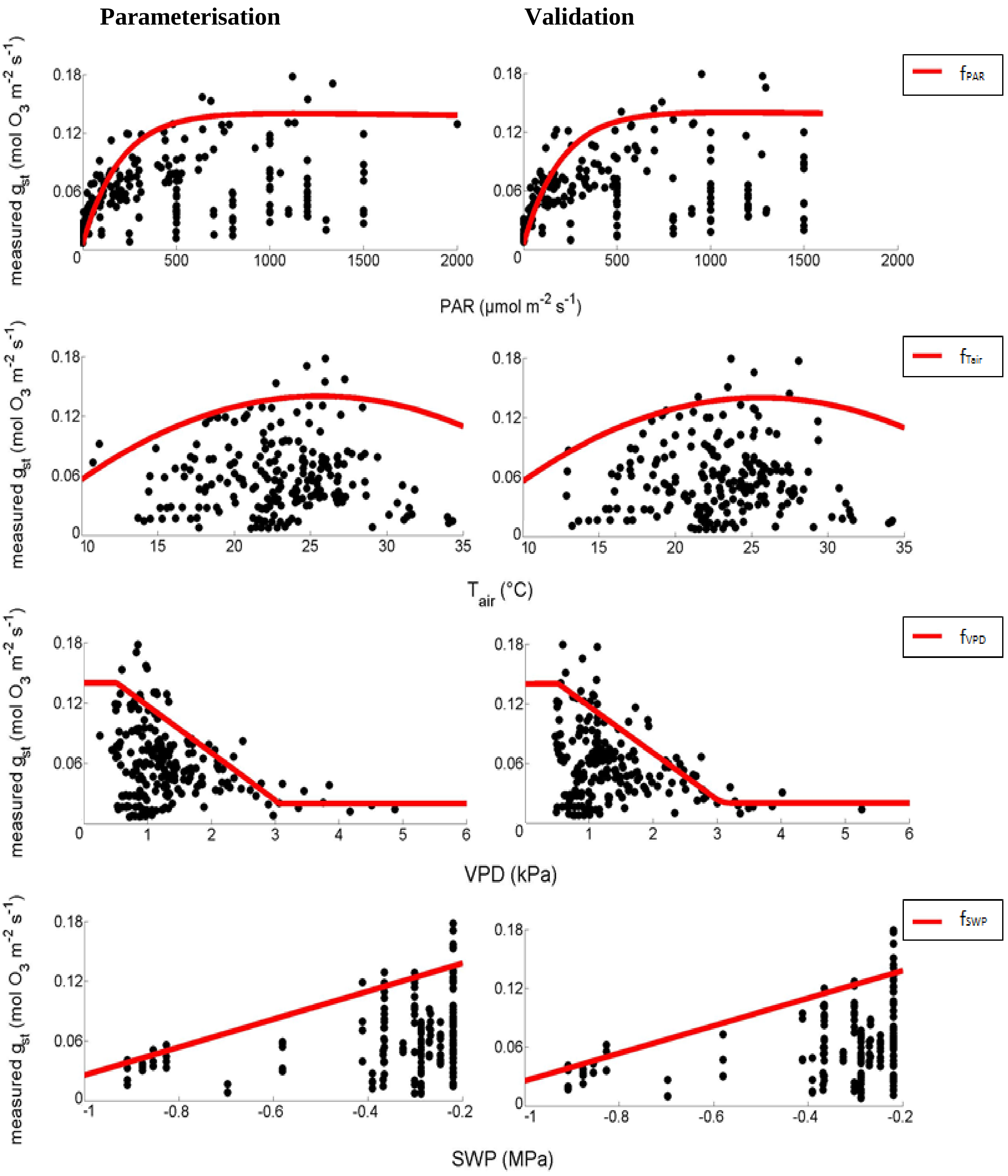

Fig. 6. Histograms of meteorological variabels for the training dataset (red) and the high O_3 uptake dataset (blue). The subplots represent global radiation R_g (A), minimum temperature T_{min} (B), maximum temperature T_{max} (C), mean temperature T_{mean} (D) and vapour pressure deficit VPD (E).

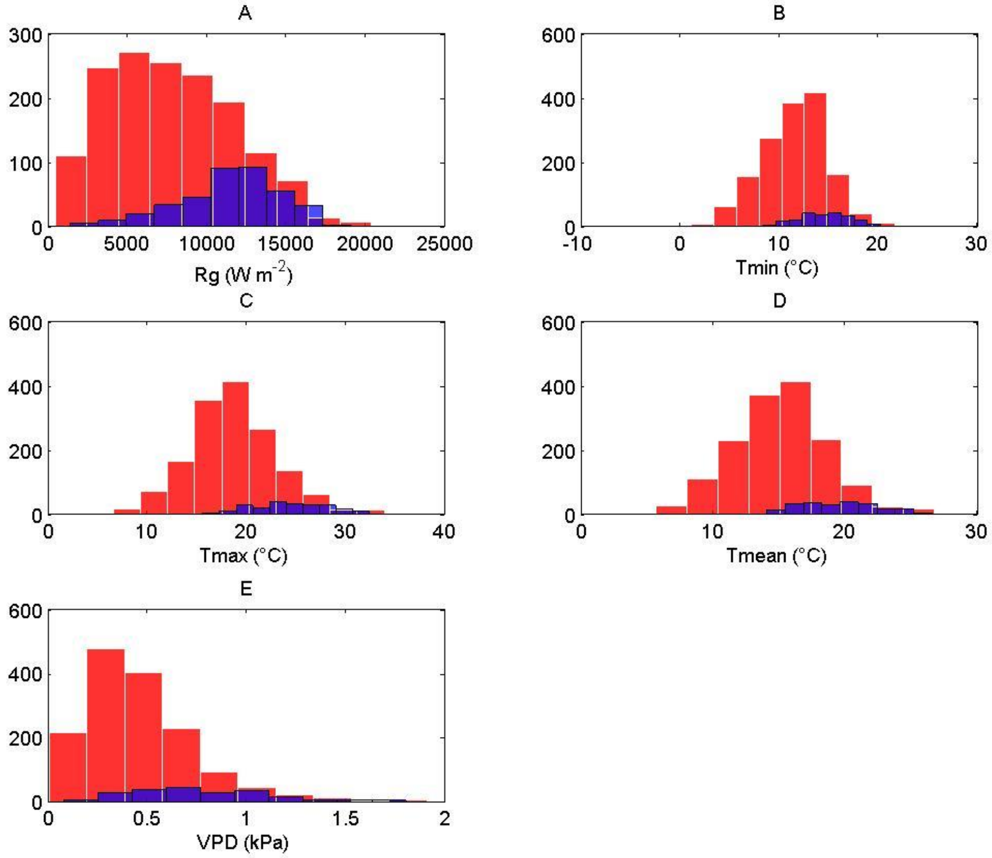

Fig. 7. Measured GPP is plotted as function of modelled GPP for two different datasets: (a) only the days before the first major O_3 peak in every year, (b) the training dataset with the days after the first major O_3 peak in every year, excluding those with high O_3 fluxes + six following days to train the network. The black line is the 1:1 line. The blue line is the regression fit including 95% confidence intervals (in grey).

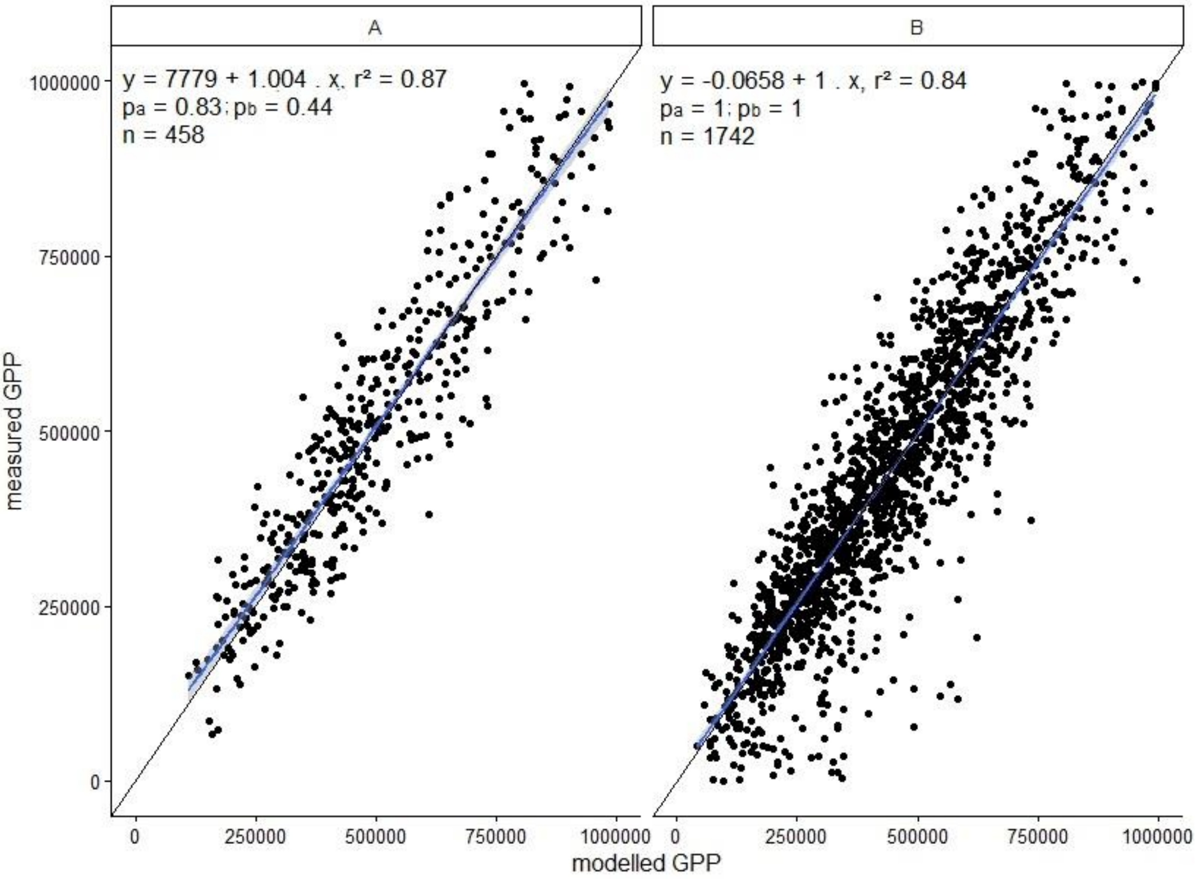

Fig. 8: Measured versus modelled gross primary productivity (GPP) for days used for model training and testing (A, B), for days on which an O_3 effect was assumed (C, D), and for the entire growing season (E, F). GPP model 1 was trained without days with the highest stomatal O_3 uptake, whereas GPP model 2 was trained to test for possible lag effects of O_3 on GPP. Black lines are fitted linear regression lines and grey lines mark the 95% confidence bands. Also shown are p-values for the tests of slope and intercept from the regression y = ax + b being different from 1 and 0, respectively. Black lines are the fitted linear regression lines and grey line are the 95% confidence bands.

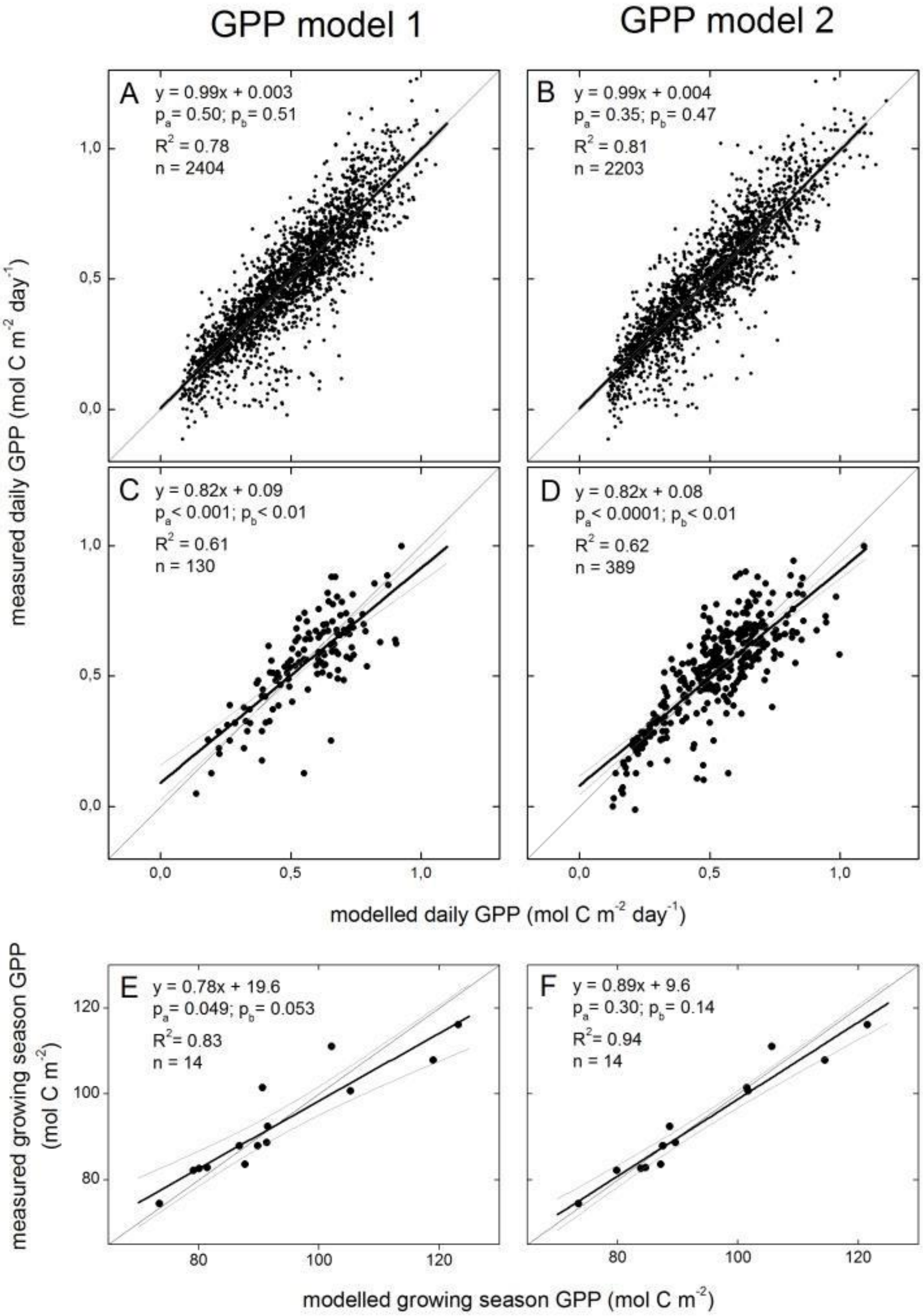

Fig. 9. Residuals of growing season gross primary productivity (GPP) in function of (A, B) total stomatal ozone flux over the growing season (F_{st}), (C, D) AOT40, and (E, F) POD_1. PLA = projected leaf area. Negative residuals indicate model overestimation of GPP. GPP model 1 was trained without days with the highest stomatal O_3 uptake, whereas GPP model 2 was trained to test for possible lag effects of O_3 on GPP. Black lines are fitted linear regression lines and grey lines mark the 95% confidence bands. Also shown are p-values for the test of the slope and intercept from the regression y=ax+b being different from 0. (n = 14).